CD155 blockade enhances allogeneic natural killer cell-mediated antitumor response against osteosarcoma

Monica M Cho[1], Longzhen Song[1], Aicha E Quamine[1], Fernanda Szewc[1], Lei Shi[1], Amy K Erbe[1,2], Jonathan D Ebben[1], David P Turicek[1], Jillian M Kline[1], Emily O Lafeber[1], Madison F Phillips[1], Amanda S Ceas[1], Paul M Sondel[1,2,3], Christian M Capitini[1,2]

[1]Department of Pediatrics, University of Wisconsin School of Medicine and Public Health, Madison, WI 53705, USA

[2]Carbone Cancer Center, University of Wisconsin School of Medicine and Public Health, Madison, WI, US 53705, USA.

[3]Department of Human Oncology, University of Wisconsin School of Medicine and Public Health, Madison, WI 53705, USA

Correspondence:

ccapitini@pediatrics.wisc.edu, Tel.: +1-608-262-2415; Fax: +1-608-265-9721

Transparency declaration

The lead author* affirms that this manuscript is an honest, accurate, and transparent account of the study being reported; that no important aspects of the study have been omitted; and that any discrepancies from the study as planned (and, if relevant, registered) have been explained.

*The manuscript's guarantor.

Availability of data and material

The datasets used and/or analyzed during the current study are available from the corresponding author on reasonable request.

Competing interests

C.M.C. reports honorarium from Bayer, Elephas, Nektar Therapeutics, Novartis and WiCell Research Institute, who had no input in the study design, analysis, manuscript preparation or decision to submit for publication. The authors declare that no other competing interests exist.

Funding

This work was supported by grants from the National Institute of General Medical Sciences/NIH T32 GM008692 and National Cancer Institute (NCI)/NIH T32 CA009135 (to MMC and JDE), NSF 1810916 WiscAMP Bridge to the Doctorate and NSF Graduate Research Fellowship Program DGE-1747503 (AEQ), NIH TL1 TR002375 (FS), NCI/NIH R35 CA197078 (to PMS), St. Baldrick's Foundation Empowering Pediatric Immunotherapy for Childhood Cancers Team grant and the Midwest Athletes Against Childhood Cancer (MACC) Fund (to PMS and CMC), NCI/NIH R01 CA215461 and an American Cancer Society Research Scholar Grant RSG-19-104-01-LIB (to CMC). The authors also thank the UWCCC Flow Cytometry core facility and Small Animal Imaging and Radiotherapy core facility, who are supported in part through NCI/NIH P30 CA014520. Figures created using BioRender.com and exported under a paid subscription. The contents of this article do not necessarily reflect the views or policies of the Department of Health and Human Services, nor does the mention of trade

names, commercial products, or organizations imply endorsement by the US Government.

Authors' contributions

MMC was responsible for experimental design, execution, and analysis of data. MMC created final versions of all figures and drafted the manuscript. LSh isolated RNA and performed quality control for microarray analysis. AEG transduced tumor cell lines with lentiviral vector. LSo, AEQ, FS, JE, DT, JK, EL, MFP, and AC contributed to experimental design and data collection. CMC provided experimental design, review of data, and thorough edits and review of the manuscript. All authors read and approved the final manuscript.

Acknowledgements

We thank the Division of Hematology, Oncology and Bone Marrow Transplant in the Department of Pediatrics and Carbone Cancer Center at the University of Wisconsin-Madison for their ongoing support. The author(s) thank the University of Wisconsin Carbone Cancer Center Flow Cytometry Laboratory, supported by P30 CA014520, Small Animal Imaging and Radiotherapy Facility, and Translational Research Initiatives in Pathology, and Biomedical Research Model Services for use of their facilities and services.

ABSTRACT

Background

Osteosarcoma (OS) patients that present with metastatic disease have a poor prognosis and no curative options. Allogeneic bone marrow transplant (alloBMT) is curative for hematologic malignancies through the graft-versus-tumor (GVT) effect, but to date has been ineffective for solid tumors like OS. CD155 is expressed on OS and interacts strongly with the inhibitory receptors TIGIT and CD96 but also binds to the activating receptor DNAM-1 on natural killer (NK) cells but has never been targeted after alloBMT. Combining adoptive transfer of allogeneic NK (alloNK) cells with CD155 checkpoint blockade after alloBMT may enhance a GVT effect against OS but could enhance toxicities like graft-versus-host-disease (GVHD).

Methods

Ex vivo activated and expanded murine NK cells were generated with soluble IL-15/IL-15Rα. AlloNK and syngeneic NK (synNK) cell phenotype, cytotoxicity, cytokine production, and degranulation against the CD155-expressing murine OS cell line K7M2 were assessed in vitro. Mice bearing pulmonary OS metastases underwent alloBMT followed by infusion of alloNK cells with combinations of anti-CD155 and anti-DNAM-1 blockade. Tumor growth, GVHD and survival were monitored and differential gene expression of lung tissue was assessed by RNA microarray.

Results

AlloNK cells exhibited superior cytotoxicity against CD155-expressing OS compared to synNK cells, and this activity was further enhanced by CD155 blockade. CD155 blockade increased alloNK cell degranulation and interferon gamma production through DNAM-1, as these functions were abrogated during DNAM-1 blockade. In vivo, CD155 blockade after alloBMT increased survival and decreased OS disease burden with no exacerbation of GVHD. Treatment with combination CD155 and DNAM-1 blockade ameliorated survival and tumor control benefits seen with CD155 blockade alone. In mice treated with CD155 blockade, genes related to NK cell cytotoxicity were upregulated. DNAM-1 blockade resulted in upregulation of NK cell inhibition and T cell function gene expression.

Conclusions

These results demonstrate the safety and efficacy of infusing alloNK cells with CD155 blockade to mount a GVT effect against OS and show benefits are in part through DNAM-1. Defining the hierarchy of receptors that govern alloNK responses will be critical to translating combination adoptive NK cell and immune checkpoint inhibition for patients with solid tumors treated with alloBMT.

WHAT IS ALREADY KNOWN ON THIS TOPIC

- Allogeneic bone marrow transplant (alloBMT) has yet to show efficacy in treating solid tumors, such as osteosarcoma (OS). CD155 is expressed on OS and interacts with natural killer (NK) cell receptors, such as activating receptor DNAM-1 and inhibitory receptors TIGIT and CD96 and has a dominant inhibitory effect on NK cell activity. Targeting CD155 interactions on allogeneic NK cells could enhance anti-OS responses, but this has not been tested after alloBMT.

WHAT THIS STUDY ADDS

- CD155 blockade enhances allogeneic natural killer cell-mediated cytotoxicity against osteosarcoma and improved overall survival and decreased tumor growth after alloBMT in an in vivo mouse model of metastatic pulmonary OS. Addition of DNAM-1 blockade abrogated CD155 blockade-enhanced allogeneic NK cell antitumor responses.

HOW THIS STUDY MIGHT AFFECT RESEARCH, PRACTICE OR POLICY

- These results demonstrate efficacy of allogeneic NK cells combined with CD155 blockade to mount an antitumor response against CD155-expressing OS. Translation of combination adoptive NK cell and CD155 axis modulation offers a platform for alloBMT treatment approaches for pediatric patients with relapsed and refractory solid tumors.

Keywords: natural killer cells, CD155, osteosarcoma, hematopoietic stem cell transplantation, DNAM-1

List of Abbreviations:

OS	osteosarcoma
NK	natural killer
KIR	killer-immunoglobulin-like receptor
MHC	major histocompatibility complex
HSCT	hematopoietic stem cell transplant
GVHD	graft-versus-host disease
GVT	graft-versus-tumor
EAE	ex vivo activation and expansion
TME	tumor microenvironment
E: T	effector: target
alloBMT	allogeneic bone marrow transplant
IFNγ	interferon gamma
MFI	median fluorescence intensity
TNF	tumor necrosis factor
synNK	syngeneic natural killer
alloNK	allogeneic natural killer
ADCC	antibody-dependent cellular cytotoxicity
Fab	antibody fragment
DGSS	directed global significance score

INTRODUCTION

Osteosarcoma (OS) is the most common primary bone cancer in children, with approximately 1,000 cases per year in the U.S. While patients with localized disease have a 5-year event free survival rate of 70%, patients with metastatic disease have only a 24% survival rate (1,2). There are no curative treatment options for patients with metastatic or relapsed/refractory disease.

Natural killer (NK) cells are innate lymphocytes that can enact cytotoxicity against tumors based on the balance between activating and inhibitory signals from cell surface receptor engagement. NK cells demonstrate self-tolerance to prevent lysis of healthy tissues through interaction between inhibitory killer-immunoglobulin-like receptors (KIRs), analogous to the Ly49 family of receptors in mice, and their ligands, self-major histocompatibility complex (MHC) class I molecules (3). Malignant cells not recognized as “self” due to KIR/Ly49 receptor mismatch are susceptible to lysis because these inhibitory receptors cannot engage MHC I ligand. Allogeneic hematopoietic stem cell transplant (alloHSCT) combined with adoptively transferred donor-derived, allogeneic NK cells is an attractive approach to augment the graft-versus-tumor (GVT) effect of NK cells generated by KIR mismatch (4). As graft-versus-host-disease (GVHD) is T-cell mediated and a major barrier in applying alloHSCT for solid tumors, there is increased interest in depleting T cells in the donor graft to reduce the risk of GVHD while administering other effector cells like NK cells post-HSCT (5,6). While several studies observe the benefit of KIR-mismatched NK cells in leukemias, more studies are needed to demonstrate KIR mismatch benefits in pediatric solid tumors (7–11).

Although allogeneic NK (alloNK) cells have great potential to treat solid tumors, there are significant barriers with respect to *in vivo* function. AlloNK cells with a KIR/KIR-ligand mismatch have not shown potent initial antitumor response due to limited function and diminished persistence. To overcome these barriers, ex vivo activated and expanded (EAE) NK cells have been used to boost antitumor effects (12). Compared to resting NK cells, EAE NK cells use multiple synergistic activating receptors and exhibit superior target cell lysis (13). EAE NK cells more effectively lyse OS cell lines and patient-derived chemotherapy-resistant OS compared to resting NK cells (14). Since IL-15 levels increase more than 10-fold during conditioning prior to HSCT and peak at 15 days post-HSCT, alloHSCT is an excellent platform for EAE alloNK cell therapy, since high levels of IL-15 support NK cell engraftment, activation and persistence. Since adoptively transferred NK cells can match the HSCT donor graft, which itself generates NK cells early post-HSCT, there is no risk of rejection (15,16).

Overcoming tumor microenvironment (TME) immunosuppression is a major barrier to successful adoptive NK cell therapy. CD155, originally discovered as the poliovirus receptor, is an immunoglobulin superfamily adhesion molecule that participates in processes including cell adhesion and migration, proliferation, and modulation of immune responses (17). Acute myeloid leukemia, multiple myeloma, neuroblastoma, fibrosarcoma, glioblastoma, melanoma, prostate cancer, renal cell cancer, pancreatic carcinomas, and colon, non-small cell lung, ovarian, breast carcinomas, and OS have all been found to express CD155 (18–21). High CD155 expression correlates with poor clinical outcomes and affects tumor susceptibility to NK cell lysis (22). DNAM-1 is a

CD155 receptor that is critical for NK cell activation due to its synergizing effect with other activation pathways, increasing actin polymerization and granule polarization (23). DNAM-1 triggers direct NK cell cytotoxicity upon interaction with CD155 and Nectin2/CD112 (24). CD155 also interacts with inhibitory receptors, TIGIT and CD96. TIGIT is an immunoglobulin superfamily receptor that is expressed on T cells and NK cells. Upon interaction with its ligands, including CD155 and CD112, TIGIT downregulates immune cell activity by attenuating NK cell degranulation, cytokine production, and cytotoxicity (25). Due to its higher affinity for CD155, TIGIT outcompetes DNAM-1, resulting in inhibitory signaling and preventing DNAM-1 signaling. CD96 also competes with DNAM-1 for CD155 binding and directly inhibits IFNγ production, activation, and cytotoxicity (26). Combining the effects of KIR/Ly49 mismatch and CD155 immune checkpoint blockade can potentially overcome TME immunosuppression to treat OS. Prior studies suggest that CD155 blockade or knockout favors NK cell antitumor effects by preventing dominant inhibitory effects, but this has not been explored in the context of alloHSCT nor in combination with adoptively transferred EAE alloNK cells (21). We hypothesized that CD155 blockade after T cell depleted alloHSCT will enhance the GVT effect of adoptively transferred EAE alloNK cells by increasing NK activation and cytotoxicity without exacerbating GVHD.

METHODS

Mice

Female C57BL/6NCr (B6) and BALB/cAnNCr (BALB/c) mice (Charles River Laboratories, Wilmington, MA) were housed in accordance with the Guide for Care and Use for Laboratory Mice. All animal experiments were performed under an IACUC approved protocol at the University of Wisconsin-Madison (M005915).

Ex vivo activation and expansion of murine NK cells

Bone marrow was harvested from 8–12-week-old female B6 or BALB/c mice and processed into a single cell suspension and red blood cells were lysed with ACK lysis buffer (Lonza, Walkersville, MD). NK cells were isolated by magnetic cell separation using negative selection with a NK cell isolation kit and an AutoMACS Pro (Miltenyi Biotec, San Jose, CA). NK cells were expanded and activated for 14 days using mouse 10 ng/ml IL-15/IL-15Rα conjugate, comprised of recombinant mouse IL-15 protein (R&D Systems, Minneapolis, MN) and recombinant mouse IL-15Ralpha Fc chimera protein (R&D Systems), in RPMI medium (Corning Life Sciences, Durham, NC) with 10% fetal bovine serum (GeminiBio, Sacramento, CA) with 50 IU/mL penicillin/streptomycin (Lonza), 0.11 mM 2-betamercaptoethanol (Gibco, Carlsbad, CA), 1X MEM nonessential amino acids (Corning), 25 mM HEPES buffer (Corning), and 1 mM sodium pyruvate (Corning). IL-15/IL-15 receptor conjugate was repleted during medium changes with half fresh and half conditioned media every 2-3 days to maintain cell concentration of 1-2 × 10^6 cells/mL. Over the 14-day expansion, freshly isolated and cultured live NK cells

were counted and analyzed by flow cytometry at days 0, 7, 9, 12 and 14. NK cells were collected 12 days post-NK cell isolation for all other in vitro and in vivo assays.

Bone marrow transplant in vivo model with adoptive NK cell transfer and antibody blockade treatment

Bone marrow cells were harvested from B6 mice and processed into single cell suspensions. A CD3ε microbead kit (Miltenyi Biotec) was used to deplete T cells from murine bone marrow cells. Recipient BALB/c mice were lethally irradiated with 8 Gy in two 4 Gy fractions using an X-Rad 320 (Precision Xray Irradiation, Madison, CT) and transplanted with 2.5-5E6 T cell-depleted B6 bone marrow cells by retroorbital injection. For an established OS disease alloHSCT model, on day 0, BALB/c mice were inoculated with 1E6 intravenous luciferase^{+} K7M2 murine OS cells. The tumor-bearing BALB/c mice underwent bone marrow transplant at day 7. For a post-HSCT relapsed disease model, BALB/c mice underwent alloBMT at day 0, followed by 1E6 intravenous luciferase^{+} K7M2 murine OS cell tumor inoculation at day 7. For both models, 7-8 days after tumor injection, mice received 1E6 allogeneic B6 EAE NK cells per mouse, expanded with IL-15/IL-15Rα for 12 days, pretreated with no antibody blockade, purified rat anti-mouse anti-DNAM-1 (Biolegend Cat. No. 128822, San Diego, CA), or purified rat anti-mouse anti-NKG2D (Biolegend Cat. No. 130202) for 30 minutes at 37°C and washed with PBS prior to retroorbital injection with concurrent intraperitoneal treatment by 200 ug of purified rat IgG2a antibody (Leinco Cat. No. I-1177, Fenton, MO) or purified rat anti-mouse anti-CD155 antibody (Leinco Cat. No. C2833).

In vivo GVHD and tumor burden monitoring and sample collection

Tumor growth in mice was monitored by bioluminescence using the IVIS Spectrum in vivo imaging system (Perkin-Elmer, Waltham, MA). Image data were analyzed using Living Image software (Perkin-Elmer, Waltham, MA). Treatment toxicity and GVHD were measured using body weight loss and GVHD clinical scoring system (27).

Statistical Analysis

Data presented show analyses of experimental replicate samples with plotted individual sample values, mean and standard error of the mean (SEM). Significance was determined by p-values $\leq$ 0.05 level. Comparisons were performed using two-sided two-sample t-tests (two experimental groups) or one-way-ANOVA/ Kruskal-Wallis with Dunn's multiple comparisons tests (greater than two experimental groups). Statistical analyses were performed using Prism 9 (Graphpad Software, San Diego, CA).

For more information, please refer to supplemental methods.

RESULTS

Expanded murine NK cells exhibit an activated phenotype

B6 and BALB/c NK cells were isolated from bone marrow and expanded with soluble IL-15/IL-15Rα complex (sIL-15/IL15Rα) for 14 days. NK cell yields per mouse post-isolation were $0.176 \pm 0.021 \times 10^6$ B6 NK cells/mouse and $0.568 \pm 0.185 \times 10^6$ BALB/c NK cells/mouse (Fig. 1A). Both B6 and BALB/c murine NK cells expanded considerably, and peak expansion was observed at day 12 with $15.92 \pm 2.91 \times 10^6$ B6 NK

cells/mouse and 7.82 ± 2.54 × 10^6 BALB/c NK cells/mouse (Fig. 1A). Maximal fold expansion occurred at day 12 with a fold expansion of 89.600 ± 13.728 for B6 NK cells and 16.988 ± 6.050 for BALB/c NK cells (Fig. 1A). At day 14, B6 and BALB/c NK cell counts fell to 2.128 ± 0.505 × 10^6 B6 NK cells/mouse and 3.560 ± 6.07 × 10^6 BALB/c NK cells/mouse (Fig. 1A).

To assess NK cell activation during expansion with sIL-15/IL15Rα, B6 and BALB/c NK cells were analyzed by flow cytometry for activating markers and death receptor expression to determine the NK cell potential to become activated and induce target cell apoptosis. During expansion, the proportion of NKG2D$^+$ cells increased, peaking at day 12, with 95.52 ± 2.654% NKG2D$^+$ B6 NK cells and 86.02 ± 4.368% NKG2D$^+$ BALB/c NK cells (Supplementary Fig. 1A-B). In B6 NK cells, %NKG2D$^+$ B6 NK cells were significantly increased at day 12 compared to pre-expansion (Supplementary Fig. 1A). Thus, sIL-15/IL15Rα both expands and activates NK cells from both strains of mice.

To evaluate cytotoxic potential, tumor necrosis factor (TNF) family members FasL and TRAIL were measured. B6 and BALB/c NK cells did not exhibit significant increases in FasL or TRAIL MFI, although the proportion of TRAIL$^+$ B6 NK cells increased at days 12 and 14 (Supplementary Fig. 1A-B). BALB/c NK cells had an initial increase in TRAIL MFI and TRAIL$^+$ NK cells at days 5 and 7, but by day 12, increased TRAIL MFI was the only persistent increase into the second week of expansion (Supplementary Fig. 1A-B).

The CD155 receptors DNAM-1, TIGIT and CD96 are expressed on mature NK cells, but it is unclear how sIL-15/IL15Rα affects their expression and if effects are strain specific. DNAM-1 MFI was significantly increased at day 12 in both B6 and BALB/c NK cells, while the proportion of DNAM-1^{+} NK cells was significantly increased in BALB/c NK cells (Supplementary Fig. 1C-D). CD96 MFI was significantly elevated in B6 and BALB/c NK cells (Supplementary Fig. 1C-D). TIGIT MFI and proportion of TIGIT^{+} NK cells were both significantly increased at day 12 of B6 NK cell expansion (Supplementary Fig. 1C-D). After 12 days of culture with sIL-15/IL15Rα, there were increased proportions of B6 NK cells expressing NKG2D, TRAIL, and TIGIT, and of BALB/c NK cells, there were greater proportions of cells expressing TRAIL and DNAM-1 (Fig. 1C). With respect to MFI fold change at day 12, murine NK cells exhibited significant increases in NKG2D, TRAIL, DNAM-1 and CD96 expression (Fig. 1D). Most significant changes in NK phenotype and proliferation coalesced on day 12 of expansion, so NK cells expanded for 12 days with sIL-15/IL15Rα were used for subsequent experiments.

CD155 blockade enhances alloreactive NK cell activity against OS

To assess murine NK cell activity against OS, we used a CD155-expressing murine K7M2 OS cell line derived from a BALB/c mouse (Fig. 2A). K7M2 had a low proportion of CD112^{+} cells (Fig. 2A). K7M2 OS was also found to express Fas and TRAIL receptor 2, which bind to apoptosis-inducing FasL and TRAIL on NK cells (Fig. 2B). To determine the contribution of Ly49 mismatch (where inhibitory Ly49 receptors on NK cells cannot see their cognate MHC I ligand) on anti-OS activity, allogeneic NK cells

from B6 mice (alloNKs) and syngeneic NK cells from BALB/c mice (synNKs) were co-cultured with K7M2 OS and evaluated for cytotoxicity using a live cell imaging system. Compared to synNKs, alloNKs showed significantly higher percentage of lysis of OS after 24 hours (alloNK 59.13 ± 3.50%, synNK 30.13 ± 3.45%) (Fig. 2C).

Blocking CD155 on OS could either enhance cytotoxicity by blocking engagement of TIGIT or CD96 on NK cells, or it could impair cytotoxicity by inhibiting engagement with DNAM-1 on NK cells. It is unclear if CD155 blockade can enhance cytotoxicity further in the setting of Ly49 mismatch. With a CD155 blocking antibody, both alloNK and synNK showed increased lysis of OS after 24 hours (Fig. 2C). Notably, alloNKs with CD155 blockade yielded the highest amount of OS lysis (98.60 ± 0.11%) and was significantly higher than OS lysis by synNKs with CD155 blockade (94.74 ± 0.37%) (Fig. 2C). Since NK cells express CD16, it is possible that blocking CD155 may inadvertently label the tumor for antibody-dependent cellular cytotoxicity (ADCC). To distinguish if alloNKs were engaging in ADCC of OS with CD155 blockade, an antibody fragment (Fab) was generated containing only the antigen binding portion of the anti-CD155 antibody without the constant region that is necessary to induce ADCC via binding to CD16 on NK cells. When compared to the full anti-CD155 antibody, the anti-CD155 Fab did not significantly affect alloNK lysis of OS, confirming that the CD155 blocking effect was not mediated by ADCC (Fig. 2D). Additionally, we observed that a CD155-expressing human OS cell line, MG63, was similarly more sensitive to human NK-92 cell mediated tumor killing with the addition of CD155 blockade, suggesting these findings are translatable to other models (Supplementary Fig 3 A-C).

Since DNAM-1 is an activating receptor on NK cells that binds CD155, we determined whether DNAM-1 was necessary for NK cell cytotoxicity against CD155-expressing OS. Blocking DNAM-1 alone did not significantly affect OS lysis by alloNKs or synNKs (Fig. 2E-F), likely because NK cells have other activating receptors to recognize tumors. However, when DNAM-1 blockade was combined with CD155 blockade, lysis of OS by alloNKs (97.63 ± 0.21%) and synNKs (93.01 ± 0.23%) was significantly decreased compared to CD155 blockade alone, though cytotoxicity remained markedly elevated compared to no blockade or DNAM-1 blockade alone (Fig. 2E-F).

We next evaluated how co-culture with CD155-expressing K7M2 OS affected cytokine production by murine NK cells. AlloNKs produced significantly more IFNγ (9.41 ± 2.18 pg/ml) compared to synNKs (4.35 ± 1.26 pg/ml) (Fig.2G). While synNK IFNγ production was not affected by DNAM-1 blockade, CD155 blockade, or combination DNAM-1 and CD155 blockade, alloNK IFNγ production was significantly increased with CD155 blockade (26.97 ± 4.79 pg/ml) compared to no blockade (Fig. 2H-I). AlloNKs with DNAM-1 blockade alone or combination DNAM-1 and CD155 blockade had significantly lower IFNγ production compared to CD155 blockade alone (Fig. 2I), implying the DNAM-1/CD155 axis is a more potent regulator of driving IFNγ production than Ly49 mismatch alloreactivity.

Next, we investigated if CD155 or DNAM-1 blockade altered NK cell cytotoxicity mechanisms. First, degranulation was assessed by measuring CD107a surface

expression on synNKs and alloNKs after incubation with K7M2 OS. AlloNKs had greater CD107a MFI and proportion of CD107a$^+$ cells compared to synNKs after incubation with K7M2 OS (Fig. 3A). With the addition of CD155 blockade, DNAM-1 blockade, or combination CD155 and DNAM-1 blockade, there were no significant differences in CD107a MFI or the proportion of CD107a$^+$ synNKs or alloNKs (Fig. 3B-C). AlloNKs also had increased perforin MFI and proportion of perforin$^+$ cells compared to synNKs, but no significant differences in granzyme B MFI or percentage of granzyme B$^+$ cells (Fig. 3D). Overall, the proportion of FasL$^+$ and TRAIL$^+$ cells were low in synNKs and alloNKs, with alloNKs having greater proportions of these cells compared to synNKs (Fig. 3E). FasL MFI was significantly lower in alloNKs compared to synNKs. There were no changes in CD107a MFI, CD107a$^+$, FasL MFI, Granzyme B MFI, FasL$^+$, or Granzyme B$^+$ in synNKs or alloNKs with CD155 axis blockade (Supplementary Fig. 2).

AlloNK treatment with CD155 blockade increases survival after alloBMT in relapsed OS

Due to superior activity observed in vitro, we then investigated whether alloNK infusion with CD155 blockade could control recurrence of pulmonary OS metastases after alloHSCT. To test this, BALB/c recipient mice underwent lethal irradiation and allogeneic bone marrow transplant (alloBMT) with T-cell-depleted B6 bone marrow since T cells compete with NK cells for cytokines like IL-15 and can cause GVHD that limits GVT effects. Seven days post-transplant, mice were inoculated with K7M2 OS injected intravenously (Fig. 4A) to mimic relapse of pulmonary metastases post-

alloBMT. Mice were then treated with EAE alloNK cell infusion given with either isotype antibody or anti-CD155 blockade.

Post-alloBMT, serum IL-15 increased (Fig. 4B). Treatment with alloNK and anti-CD155 blockade significantly increased overall survival compared to alloNK with isotype control (Fig. 4C). Tumor burden measured by bioluminescence showed significantly decreased tumor growth at days 10 and 14 post-tumor inoculation in mice treated with CD155 blockade compared to isotype control (Fig. 4E). EAE NK cell infusions after alloBMT have been associated with exacerbating GVHD in humans (28). There were no significant differences in clinical GVHD scores between mice treated with isotype antibody or anti-CD155 blockade (Fig. 4D). Thus, anti-CD155 antibody does not exacerbate GVHD from residual T cells in the donor graft, graft-derived de novo T cells or EAE alloNK infusion.

To determine the role of DNAM-1 on the in vivo effects of CD155 blockade, EAE alloNK cells pre-incubated with anti-DNAM-1 blocking antibody were infused with either an isotype antibody or anti-CD155 blockade into mice with pulmonary OS metastases after alloBMT. Anti-DNAM-1 blockade did not significantly impact tumor growth compared to isotype control or anti-CD155 blockade (Fig. 4F). Anti-DNAM-1 blockade in combination with anti-CD155 blockade abrogated decreased tumor growth seen with anti-CD155 blockade alone (Fig. 4F). Thus, combination of DNAM-1 and CD155 blockade worsened antitumor responses, implying DNAM-1 contributes to anti-tumor activity of pulmonary OS after alloBMT.

Combination alloBMT, alloNK treatment and CD155 blockade does not control established pulmonary OS disease

We then tested the efficacy of treating established pulmonary OS metastases with T-cell-depleted alloBMT followed by EAE alloNK cells and anti-CD155 blockade. BALB/c mice were inoculated with K7M2 OS injected intravenously (Fig. 5A). Mice were then treated with an alloBMT using T-cell-depleted B6 bone marrow cells at day 7, followed by EAE alloNK cells infusion and isotype control or anti-CD155 blocking antibody on day 8. Post-alloBMT, again serum levels of IL-15 increased (Fig. 5B). There was no significant survival benefit or decreased tumor growth in mice treated with anti-CD155 blockade compared to mice treated with alloNKs and isotype antibody (Fig. 5C). Anti-CD155 blockade in this model also did not exacerbate GVHD (Fig. 5D). When alloNKs were infused in the setting of anti-DNAM-1 blockade, there was no significant difference in survival or OS disease progression when compared to mice receiving isotype control or anti-CD155 blockade (Fig. 5C, E). The combination of anti-CD155 and anti-DNAM-1 blockade resulted in lower overall survival compared to the other treatment groups (Fig. 5C). Unlike treating relapsed disease after alloBMT, treatment of established pulmonary OS metastases with alloBMT followed by alloNK cells and CD155 blockade did not significantly impact survival or pulmonary OS progression, and blocking DNAM-1 on NK cells exacerbated lethality.

Gene regulation effects of combination alloBMT, alloNK and CD155 axis blockade in vivo

To investigate tumor microenvironment changes of the established pulmonary OS metastases model that may explain its resistance to alloBMT and alloNK therapy, we performed RNA microarray analysis on lung tissue isolated from OS tumor-bearing mice treated with alloNK and either IgG2a isotype or anti-CD155 antibody. There were 6 genes with an absolute fold change greater than or equal to 2-fold with an adjusted p-value < 0.05 (Fig. 7A). Among genes with an absolute fold change greater than or equal to 2, 5 genes were upregulated, and 1 gene was downregulated (Fig. 6B).

Genes associated with increased NK and other immune effector activity were upregulated. *Prf1*, *Klrk1*, and *Hcst* were upregulated in CD155-blockade treated mice (Fig. 6B). Prf1, encoding perforin 1, was upregulated in the CD155 blockade treated mice with a 2.20225-fold increase (p value = 0.012281). Killer cell lectin-like receptor subfamily K (*Klrk1*) encoding NKG2D had a 2.15217-fold change (p value = 0.04821). Hematopoietic cell signal transducer (*Hcst)* encoding DAP10 had a 2.78557-fold change (p value = 0.004467). In the gene set enrichment analysis, the directed global significance score (DGSS) was 1.592 for NK cell function (*Klrk1*, *Il2rb*, *Ccl3*, *Ccl5*) (Fig. 6B).

In addition, *Cma1* was upregulated (Fig. 6B). *Cma1* encodes chymase 1, which is produced by mast cells, and is associated with tumor immune escape (29). *Ciita*, or class I transactivator, is a master transcriptional regulator of MHC class II and was found to be downregulated in lung tissue from CD155 blockade treated mice with a fold change of -2.15254 (p value = 0.016355). It acts indirectly on MHC II gene promoters and loss of MHC II is associated with immune escape. Despite Cma1 upregulation, the

DGSS for cancer progression was -1.0644 (Fig. 6C). For the interferon pathway (Ciita), the DGSS was -0.9878 (Fig. 6C).

In mice treated with DNAM-1 blockade, genes related to NK cell function were upregulated relative to mice treated with isotype control (Fig. 6E). Various Ly49 receptors, analogous to human KIRs, were found to be upregulated in the DNAM-1 blockade treated mice. *Klra17* (Ly49Q) had a fold change of 3.10937 (p value = 0.029683), *Klra7* (Ly49G) had a fold change of 3.2 (p value = 0.006998), *Klrc1* (NKG2A) had a fold change of 3.49999 (p value of 0.009645), *Klrc2* (NKG2C) had a fold change of 3.56522 (p value = 0.007924), *Klrd1* (CD94) had a fold change of 3.63637 (p-value = 0.001779), and *Klra6* (Ly49F) had a fold change of 3.19446 (p value = 0.004714). *H60a*, which encodes the NKG2D ligand H60, was found to be upregulated after DNAM-1 blockade with a fold change of 2.36264 (p value = 0.039681). Mice treated with DNAM-1 blockade also exhibited changes in gene expression related to decreased NK cell activation. *2B4* was downregulated with a decreased fold change of -2.09644 (p-value = 0.000427). *TIGIT* was also significantly upregulated, increasing by fold change 5.54839 (p value = 0.0081). The myriad of changes related to NK cells was reflected in the gene set enrichment analysis, with a DGSS of 0.9998 for NK cell function (*cd244*, *slamf7*, *klra17*, *klra7*, *cd247*, *h60a*, *klrd1*, *il21b*, *ccl7*, *klra6*, *cd7*, *il12a*, *klrc1*) (Fig. 6G).

Changes in differential gene expression in mice treated with DNAM-1 blockade indicated a role for modulating T cell responses (Fig. 6F). Various tumor necrosis factor (TNF) superfamily members were upregulated in lung tissue of DNAM-1 treated mice. *Tnfsf18* was upregulated with a fold change of 7.40002 (p value = 0.021843). *Tnfsf18* is known as GITR or activation inducible TNFR family member

(AITR), a type I transmembrane protein that is expressed at high levels on $CD4^+CD25^+$ regulatory T cells (Tregs) and on B, NK, NKT cells, granulocytes and macrophages (30). *Tnfrs9* was significantly upregulated in DNAM-1 treated mouse lung tissue with a fold change of 7.14285 (p value = 0.003173). *Tnfs14* or LIGHT is another TNF super family member implicated in antitumor effects that was found to be upregulated with a fold change of 7.25643 (p value = 0.003303). Changes in the TNF superfamily pathway had a DGSS of 1.4705 (*tnfsf18*, *tnfrsf9*, *tnfsf14*, *cd40lg*, *cd70*) (Fig. 6G).

DNAM-1 blockade has more potent inhibitory effects compared to NKG2D blockade

Due to changes noted in NKG2D-related genes in the setting of DNAM-1 blockade, murine synNK and alloNK cells were co-cultured with K7M2 OS in the presence of DNAM-1 blocking antibody and evaluated for NKG2D expression. AlloNK cells had higher NKG2D MFI and proportion of $NKG2D^+$ NK cells compared to synNK cells (Fig. 7A). SynNKs had markedly increased NKG2D expression and proportion of $NKG2D^+$ NK cells when co-cultured with K7M2 OS with DNAM-1 and CD155 blockade combined compared to isotype control, and the combination of DNAM-1 and CD155 blockade significantly increased $NKG2D^+$ NK cells compared to CD155 blockade alone (Fig. 7B). In alloNKs, DNAM-1 blockade alone increased NKG2D MFI and $NKG2D^+$ NK cells compared to isotype control and CD155 blockade alone (Fig. 7B). To see if NKG2D upregulation augmented cytotoxicity, alloNK cells were tested for cytotoxicity against K7M2 OS with anti-DNAM-1, anti-NKG2D, and anti-CD155 blockade. While DNAM-1 blockade could significantly decrease tumor lysis when combined with anti-NKG2D,

NKG2D blockade did not significantly change tumor lysis when added to CD155 blockade (Fig. 7C). These data indicate that DNAM-1 is a more potent regulator of alloNK cell anti-OS responses compared to NKG2D.

DISCUSSION

In this work, EAE murine NK cells showed significant expansion with changes in both activating and inhibitory receptors. After sIL-15/IL15Rα expansion, DNAM-1 expression on EAE murine NK cells increased, peaking at day 12. The proportion of TRAIL expressing cells also increased during expansion. Although CD96 expression increased and may contrast with increased activation markers, recent work suggests CD96 also activates NK cells by mediating adhesion to CD155-expressing cells (31). Overall, these changes mediated by sIL-15/IL15Rα expansion yielded a favorable phenotype at day 12 with cytotoxic potential.

With respect to translatability to humans, human immunoglobulin-like receptors (KIRs) and murine Ly49 receptor family have distinct structures. Both receptor types exhibit polymorphic and polygenic heterogeneity and serve analogous functions (32). In addition, activating receptor ligands differ by species as human NKG2D binds MICA, MICB, and ULBP family members, but murine NKG2D binds Rae-1 family members, MULT1, and H60 isoforms (33). Freshly isolated murine NK cells also exhibit weaker lytic activity compared to freshly isolated human NK cells, although this depends on culture and stimulation conditions (34). Therefore, murine NK cell findings must be validated in human preclinical NK cells. We demonstrated that a CD155-expressing human OS cell line was more susceptible to NK-cell-mediated lysis with the addition of CD155 blockade (Supplementary Fig 3 A-C). These preliminary data show potential for translation, but further work is needed with xenograft and humanized models.

AlloNKs demonstrated greater degranulation and increased perforin expression compared to synNKs, suggesting that Ly49 receptor mismatch impacts NK cell-mediated cytotoxicity. Granule exocytosis was impaired in synNKs, likely due to self-MHC recognition on OS. While FasL and TRAIL expression are increased in activated, mature NK cells, few EAE synNK or alloNK cells expressed these ligands after stimulation with CD155-expressing OS. In interpreting these findings, it is critical to consider the kinetics of degranulation versus death receptor-mediated apoptosis. Degranulation and death receptor-mediated cytotoxicity can occur simultaneously and synergize. However, granule-mediated events happen on a shorter timescale and dominate early in target cell engagement. In contrast, FasL and TRAIL require more time to increase in surface concentration prior to killing events (35). NK cells only require 1% of granule release to kill a single target cell, and this efficiency allows NK cells to kill targets without releasing a large portion of stored granules (35).

While CD155 blockade enhanced NK cell cytotoxicity and IFNγ production against OS, combination CD155 and DNAM-1 blockade did not affect degranulation or death receptor expression in NK cells or affect IFNγ production by synNK cells. These results demonstrate that inhibition through self-recognition regulates receptor expression independent of cytokine production. Blocking DNAM-1 does not significantly affect immune control of OS by synNKs, as observed by others, (23), and we showed similar findings in that DNAM-1 blockade alone did not significantly affect alloNK cytotoxicity, IFNγ production, or degranulation compared to no blockade. The K7M2 OS cell line has low expression of CD112 (Fig. 3A), which also interacts with DNAM-1 and TIGIT.

Therefore, our model was limited in assessing the role of CD112 and its relation to alloreactivity.

Blocking CD155 could either interfere with engagement of the activating receptor DNAM-1 on NK cells, leading to larger tumors, or interfere with engagement of the inhibitory receptors TIGIT or CD96 on NK cells, leading to smaller tumors. We evaluated the efficacy of CD155 blockade combined with alloNKs after alloBMT to treat two scenarios of pulmonary OS. First, we treated mice with relapsed pulmonary OS disease after alloBMT. These results showed that the combination of anti-CD155 antibody and alloNKs improves overall survival and controls tumor growth in relapsed disease, perhaps interfering with TIGIT or CD96 inactivation of NK cells. The CD155 axis affects graft tolerance due to CD155 expressed by dendritic cells (DCs) interacting with DNAM-1 and TIGIT on alloreactive donor T cells. TIGIT-Fc fusion protein that binds to CD155 and activates signaling on DCs has been shown to reduce acute GVHD symptoms (36). In addition, DCs upregulate CD155 in the setting of acute GVHD (36). Importantly, CD155 blockade or DNAM-1 blockade did not exacerbate GVHD in the setting of alloBMT and alloNK infusion.

While alloBMT with adoptively transferred alloNK and CD155 blockade improved survival against OS relapse, it was unsuccessful in treating established disease. We explored differential gene expression of mice with established disease treated with alloBMT, alloNKs, and CD155 blockade. Gene expression upregulation of *Prf1*, *Klrk1* (NKG2D), and *Hcst* (DAP10) in CD155 blockade-treated mice showed increased

immune cell effector activity. NKG2D associates with DAP10, which recruits p85 PI3 kinase and Vav-1 signaling complex (37). These interactions mobilize Ca^{2+} and activate cytotoxicity against target cells (38). While NKG2D synergizes with other activating receptors like 2B4, it does not synergize with DNAM-1 (38). When DNAM-1 is blocked, NKG2D may mediate NK cell antitumor effects. *H60a*, which encodes a potent NKG2D ligand, was upregulated and has been found to recruit NK cells and sensitize tumors to rapid NK cell-mediated elimination (39). Interestingly, NKG2D expression increased in the setting of DNAM-1 blockade on synNKs and alloNKs. Thus, in tumors expressing NKG2D ligands, antitumor response impairment through DNAM-1 signaling could be compensated by NKG2D pathway upregulation. Blocking NKG2D did not significantly abrogate CD155-enahnced alloNK cell-mediated anti-OS cytotoxicity, unlike DNAM-1 blockade (Fig. 7D). Thus, in this context, DNAM-1 is a more potent regulator of NK cell cytotoxicity compared to the NKG2D pathway. Further studies into regulation of the DNAM-1 and NKG2D pathways may elucidate their relative activity in the setting of immune checkpoint blockade.

In addition to evidence of antitumor effects, gene expression changes in lung tissue of mice receiving CD155 blockade treatment pointed towards pro-oncogenic factors and immune escape mechanisms. Chymase is responsible for angiotensin II production which promotes vascular endothelial growth factor (VEGF) angiogenesis (40). Chymase-expressing mast cells correlate with microvessel formation, disease progression, and poor prognosis in gastric cancer, oral squamous cell carcinoma, lung cancer, and lung colonization by melanoma (41–43). In small cell lung cancer, tumors

exhibit loss of *ciita* and, consequently, loss of MHC Class II and deficient HLA-DR expression (44). Thus, loss or downregulation of *Ciita* may allow tumor to escape anti-cancer immunity. Various genes for NK inhibitory receptors, like Ly49F and NKG2A were upregulated in mice treated with DNAM-1 blockade. Two receptors that form heterodimers with CD94 were found to be upregulated in mice receiving DNAM-1 blockade. *Klrd1* encodes CD94 with forms a heterodimer with NKG2A, an inhibitory receptor encoded by *klrc1* that recognizes non-classical class I molecule HLA-E in humans and Qa-1b in mice (45). NKG2A/CD94 interaction with HLA-E causes ITIM phosphorylation and SHP-1 recruitment to suppress effector functions (46). The upregulation of inhibitory Ly49 molecules and NKG2A in the setting of DNAM-1 blockade implies that DNAM-1 may regulate inhibitory receptor expression. Thus, strategies that prevent Ly49 inhibitory receptor engagement, such as alloHSCT and/or alloNK infusions, and maximize DNAM-1 expression may skew NK cells to maximal activation against OS.

In conclusion, we have found evidence that CD155 blockade in concert with adoptively transferred alloNK cells significantly impacts the immune response against CD155-expressing pulmonary OS that relapses after alloBMT. Clinical trials incorporating α/β T cell depletion alloHSCT as a means of depleting GVHD-causing α/β T cells while enriching the donor graft with GVT-promoting γ/δ T cells and NK cells are underway, including for children with OS (NCT02508038). A pilot trial testing EAE alloNK infusions in non-transplanted OS patients is also underway (NCT03209869) (47). These findings demonstrate that carefully rebuilding the immune system after alloHSCT using adoptive

cell therapy and CD155 axis modulation is a potential immunotherapy approach for controlling relapse of metastatic solid tumors like OS.

REFERENCES

1. Luetke A, Meyers PA, Lewis I, Juergens H. Osteosarcoma treatment - where do we stand? A state of the art review. Cancer Treat Rev. 2014 May;40(4):523–32.

2. Kager L, Zoubek A, Pötschger U, Kastner U, Flege S, Kempf-Bielack B, et al. Primary metastatic osteosarcoma: presentation and outcome of patients treated on neoadjuvant Cooperative Osteosarcoma Study Group protocols. J Clin Oncol Off J Am Soc Clin Oncol. 2003 May 15;21(10):2011–8.

3. Kim S, Poursine-Laurent J, Truscott SM, Lybarger L, Song YJ, Yang L, et al. Licensing of natural killer cells by host major histocompatibility complex class I molecules. Nature. 2005 Aug 4;436(7051):709–13.

4. Quamine AE, Olsen MR, Cho MM, Capitini CM. Approaches to Enhance Natural Killer Cell-Based Immunotherapy for Pediatric Solid Tumors. Cancers. 2021 Jun 4;13(11):2796.

5. Bachanova V, Cooley S, Defor TE, Verneris MR, Zhang B, McKenna DH, et al. Clearance of acute myeloid leukemia by haploidentical natural killer cells is improved using IL-2 diphtheria toxin fusion protein. Blood. 2014 Jun 19;123(25):3855–63.

6. Ruggeri L, Capanni M, Urbani E, Perruccio K, Shlomchik WD, Tosti A, et al. Effectiveness of donor natural killer cell alloreactivity in mismatched hematopoietic transplants. Science. 2002 Mar 15;295(5562):2097–100.

7. Calvo T, Reina-Ortiz C, Giraldos D, Gascón M, Woods D, Asenjo J, et al. Expanded and activated allogeneic NK cells are cytotoxic against B-chronic lymphocytic leukemia (B-CLL) cells with sporadic cases of resistance. Sci Rep. 2020 Nov 10;10(1):19398.

8. Meazza R, Falco M, Loiacono F, Canevali P, Della Chiesa M, Bertaina A, et al. Phenotypic and Functional Characterization of NK Cells in αβT-Cell and B-Cell Depleted Haplo-HSCT to Cure Pediatric Patients with Acute Leukemia. Cancers. 2020 Aug 5;12(8):2187.

9. Nguyen R, Wu H, Pounds S, Inaba H, Ribeiro RC, Cullins D, et al. A phase II clinical trial of adoptive transfer of haploidentical natural killer cells for consolidation therapy of pediatric acute myeloid leukemia. J Immunother Cancer. 2019 Mar 20;7(1):81.

10. Rubnitz JE, Inaba H, Kang G, Gan K, Hartford C, Triplett BM, et al. Natural killer cell therapy in children with relapsed leukemia. Pediatr Blood Cancer. 2015 Aug;62(8):1468–72.

11. Lee DA, Denman CJ, Rondon G, Woodworth G, Chen J, Fisher T, et al. Haploidentical Natural Killer Cells Infused before Allogeneic Stem Cell Transplantation for Myeloid Malignancies: A Phase I Trial. Biol Blood Marrow Transplant J Am Soc Blood Marrow Transplant. 2016 Jul;22(7):1290–8.

12. Miller JS, Soignier Y, Panoskaltsis-Mortari A, McNearney SA, Yun GH, Fautsch SK, et al. Successful adoptive transfer and in vivo expansion of human haploidentical NK cells in patients with cancer. Blood. 2005 Apr 15;105(8):3051–7.

13. Bryceson YT, March ME, Ljunggren HG, Long EO. Synergy among receptors on resting NK cells for the activation of natural cytotoxicity and cytokine secretion. Blood. 2006 Jan 1;107(1):159–66.

14. Chauvin JM, Ka M, Pagliano O, Menna C, Ding Q, DeBlasio R, et al. IL15 Stimulation with TIGIT Blockade Reverses CD155-mediated NK-Cell Dysfunction in Melanoma. Clin Cancer Res Off J Am Assoc Cancer Res. 2020 Oct 15;26(20):5520–33.

15. Melenhorst JJ, Tian X, Xu D, Sandler NG, Scheinberg P, Biancotto A, et al. Cytopenia and leukocyte recovery shape cytokine fluctuations after myeloablative allogeneic hematopoietic stem cell transplantation. Haematologica. 2012 Jun;97(6):867–73.

16. Russo A, Oliveira G, Berglund S, Greco R, Gambacorta V, Cieri N, et al. NK cell recovery after haploidentical HSCT with posttransplant cyclophosphamide: dynamics and clinical implications. Blood. 2018 Jan 11;131(2):247–62.

17. Molfetta R, Zitti B, Lecce M, Milito ND, Stabile H, Fionda C, et al. CD155: A Multi-Functional Molecule in Tumor Progression. Int J Mol Sci. 2020 Jan 30;21(3):922.

18. Castriconi R, Dondero A, Corrias MV, Lanino E, Pende D, Moretta L, et al. Natural killer cell-mediated killing of freshly isolated neuroblastoma cells: critical role of DNAX accessory molecule-1-poliovirus receptor interaction. Cancer Res. 2004 Dec 15;64(24):9180–4.

19. Sloan KE, Eustace BK, Stewart JK, Zehetmeier C, Torella C, Simeone M, et al. CD155/PVR plays a key role in cell motility during tumor cell invasion and migration. BMC Cancer. 2004 Oct 7;4:73.

20. Casado JG, Pawelec G, Morgado S, Sanchez-Correa B, Delgado E, Gayoso I, et al. Expression of adhesion molecules and ligands for activating and costimulatory receptors involved in cell-mediated cytotoxicity in a large panel of human melanoma cell lines. Cancer Immunol Immunother CII. 2009 Sep;58(9):1517–26.

21. Zhuo B, Li Y, Gu F, Li Z, Sun Q, Shi Y, et al. Overexpression of CD155 relates to metastasis and invasion in osteosarcoma. Oncol Lett. 2018 May;15(5):7312–8.

22. Gao J, Zheng Q, Xin N, Wang W, Zhao C. CD155, an onco-immunologic molecule in human tumors. Cancer Sci. 2017 Oct;108(10):1934–8.

23. Zhang Z, Wu N, Lu Y, Davidson D, Colonna M, Veillette A. DNAM-1 controls NK cell activation via an ITT-like motif. J Exp Med. 2015 Nov 16;212(12):2165–82.

24. de Andrade LF, Smyth MJ, Martinet L. DNAM-1 control of natural killer cells functions through nectin and nectin-like proteins. Immunol Cell Biol. 2014 Mar;92(3):237–44.

25. Chauvin JM, Zarour HM. TIGIT in cancer immunotherapy. J Immunother Cancer. 2020 Sep;8(2):e000957.

26. Chan CJ, Martinet L, Gilfillan S, Souza-Fonseca-Guimaraes F, Chow MT, Town L, et al. The receptors CD96 and CD226 oppose each other in the regulation of natural killer cell functions. Nat Immunol. 2014 May;15(5):431–8.

27. Cooke KR, Kobzik L, Martin TR, Brewer J, Delmonte J, Crawford JM, et al. An experimental model of idiopathic pneumonia syndrome after bone marrow transplantation: I. The roles of minor H antigens and endotoxin. Blood. 1996 Oct 15;88(8):3230–9.

28. Shah NN, Baird K, Delbrook CP, Fleisher TA, Kohler ME, Rampertaap S, et al. Acute GVHD in patients receiving IL-15/4-1BBL activated NK cells following T-cell-depleted stem cell transplantation. Blood. 2015 Jan 29;125(5):784–92.

29. Takai S, Jin D. Pathophysiological Role of Chymase-Activated Matrix Metalloproteinase-9. Biomedicines. 2022 Oct 7;10(10):2499.

30. Placke T, Kopp HG, Salih HR. Glucocorticoid-induced TNFR-related (GITR) protein and its ligand in antitumor immunity: functional role and therapeutic modulation. Clin Dev Immunol. 2010;2010:239083.

31. Feng S, Isayev O, Werner J, Bazhin AV. CD96 as a Potential Immune Regulator in Cancers. Int J Mol Sci. 2023 Jan 9;24(2):1303.

32. Rahim MMA, Tu MM, Mahmoud AB, Wight A, Abou-Samra E, Lima PDA, et al. Ly49 receptors: innate and adaptive immune paradigms. Front Immunol. 2014;5:145.

33. Mestas J, Hughes CCW. Of mice and not men: differences between mouse and human immunology. J Immunol Baltim Md 1950. 2004 Mar 1;172(5):2731–8.

34. Hébert P, Pruett SB. Selective loss of viability of mouse NK cells in culture is associated with decreased NK cell lytic function. In Vitr Mol Toxicol. 2001;14(2):71–82.

35. Ramírez-Labrada A, Pesini C, Santiago L, Hidalgo S, Calvo-Pérez A, Oñate C, et al. All About (NK Cell-Mediated) Death in Two Acts and an Unexpected Encore: Initiation, Execution and Activation of Adaptive Immunity. Front Immunol. 2022;13:896228.

36. Zhang D, Hu W, Xie J, Zhang Y, Zhou B, Liu X, et al. TIGIT-Fc alleviates acute graft-versus-host disease by suppressing CTL activation via promoting the generation of immunoregulatory dendritic cells. Biochim Biophys Acta Mol Basis Dis. 2018 Sep;1864(9 Pt B):3085–98.

37. Lanier LL. NKG2D receptor and its ligands in host defense. Cancer Immunol Res. 2015 Jun;3(6):575–82.

38. Kwon HJ, Kim HS. Signaling for Synergistic Activation of Natural Killer Cells. Immune Netw. 2012 Dec;12(6):240–6.

39. Diefenbach A, Jensen ER, Jamieson AM, Raulet DH. Rae1 and H60 ligands of the NKG2D receptor stimulate tumour immunity. Nature. 2001 Sep 13;413(6852):165–71.

40. Kurihara Shimomura M, Sasahira T, Shimomura H, Bosserhoff AK, Kirita T. Mast cell chymase promotes angiogenesis and lymphangiogenesis mediated by activation of melanoma inhibitory activity gene family members in oral squamous cell carcinoma. Int J Oncol. 2020 May 1;56(5):1093–100.

41. Kondo K, Muramatsu M, Okamoto Y, Jin D, Takai S, Tanigawa N, et al. Expression of chymase-positive cells in gastric cancer and its correlation with the angiogenesis. J Surg Oncol. 2006 Jan 1;93(1):36–42; discussion 42-43.

42. Ibaraki T, Muramatsu M, Takai S, Jin D, Maruyama H, Orino T, et al. The relationship of tryptase- and chymase-positive mast cells to angiogenesis in stage I non-small cell lung cancer. Eur J Cardio-Thorac Surg Off J Eur Assoc Cardio-Thorac Surg. 2005 Oct;28(4):617–21.

43. Öhrvik H, Grujic M, Waern I, Gustafson AM, Ernst N, Roers A, et al. Mast cells promote melanoma colonization of lungs. Oncotarget. 2016 Oct 18;7(42):68990–9001.

44. Yazawa T, Kamma H, Fujiwara M, Matsui M, Horiguchi H, Satoh H, et al. Lack of class II transactivator causes severe deficiency of HLA-DR expression in small cell lung cancer. J Pathol. 1999 Jan;187(2):191–9.

45. Borrego F, Masilamani M, Kabat J, Sanni TB, Coligan JE. The cell biology of the human natural killer cell CD94/NKG2A inhibitory receptor. Mol Immunol. 2005 Feb;42(4):485–8.

46. Dutta S, Ganguly A, Chatterjee K, Spada S, Mukherjee S. Targets of Immune Escape Mechanisms in Cancer: Basis for Development and Evolution of Cancer Immune Checkpoint Inhibitors. Biology. 2023 Jan 30;12(2):218.

47. Damodharan SN, Walker KL, Forsberg MH, McDowell KA, Bouchlaka MN, Drier DA, et al. Analysis of ex vivo expanded and activated clinical-grade human NK cells after cryopreservation. Cytotherapy. 2020 Aug;22(8):450–7.

Figure 1. IL-15 expansion of murine NK cells results in activated murine NK. B6 and BALB/c NK cells cultured with IL-15/IL-15Rα conjugate with additional media and cytokine repletion every 2-3 days are shown. (A) Cell count and (B) fold expansion at days 0, 7. 9, 12, and 14. Percentage of (A) B6 and BALB/c NK cells with marker expression at day 0 and day 12 shown with individual experimental replicates plotted with mean and SEM. (C) Fold change of marker expression MFI at day 12 compared to day 0 shown for B6 NK cells and BALB/c NK cells. Mean with SEM shown for experimental replicates (n = 5). Two-sided two-sample t tests were performed (* $p < 0.05$, ** $p < 0.01$, *** $p < 0.001$, **** $p > 0.0001$).

Figure 2: AlloNKs exhibit potent anti-OS activity enhanced by CD155 blockade. (A) Proportion of K7M2 OS expressing CD155 and CD112 shown (B) Proportion of K7M2 OS expressing Fas and TRAIL R2 shown. Individual values (n = 5) plotted with mean and SEM. EAE murine alloNK and synNK were plated with mKate2-expressing K7M2 OS at an effector: target ratio of 2.5:1 with or without anti-CD155 antibody in the presence of green fluorescent caspase 3/7-substrate. Green and red fluorescence objects were measured by Incucyte real-time analysis. %Lysis was calculated based on target alone and staurosporine-induced max lysis conditions. OS lysis shown for (C) alloNK and synNK with or without anti-CD155 antibody blockade at E:T 2.5:1 (n = 5 per group), (D) alloNK with anti-CD155 antibody or anti-CD155 Fab at E:T 2:1 (n = 3 per group), (E) synNK with anti-CD155, anti-DNAM-1, or anti-CD155 and anti-DNAM-1 blockade at E:T 2.5:1 (n = 5 per group), and (F) alloNK with anti-CD155, anti-DNAM-1, or anti-CD155 and anti-DNAM-1 blockade at E:T 2.5:1 (n = 5 per group). Supernatant was collected and analyzed for IFNγ release by ELISA with samples in triplicate. Concentration was calculated based on 5 parameter curve fit interpolated from standard curve. IFNγ concentration shown for (G) alloNK and synNK (H) synNK with anti-CD155, anti-DNAM-1, or anti-CD155 and anti-DNAM-1 blockade, and (I) alloNK with anti-CD155, anti-DNAM-1, or anti-CD155 and anti-DNAM-1 blockade. Mean with SEM shown for technical replicates. Two-sided two-sample t tests and one-way ANOVA and Kruskal-Wallis with Dunn's multiple comparisons tests were performed (* $p < 0.05$, ** $p < 0.01$, *** $p < 0.001$, **** $p < 0.0001$).

Figure 3: Degranulation is the main killing mechanism used by alloNKs against OS. EAE murine alloNK and synNK cells were plated with K7M2 OS at an E:T ratio of 2.5:1. Cells were incubated for 30 minutes, followed by addition of monesin and brefeldin A, and incubated for an additional 4 hours. NK cells were collected, fixed and permeabilized, stained with surface antibodies and analyzed by flow cytometry. Cells were gated on B6 ($NK1.1^+$) and BALB/c ($CD49b^+$) cells and CD107a MFI was calculated and gated on $CD107a^+$ cells $perforin^+$, granzyme B^+, $FasL^+$, and $TRAIL^+$ cells. CD107a MFI and percentage of cells expressing CD107a for alloNK and synNK cells (A), synNK cells with CD155 axis blockade (B), and alloNK cells with CD155 axis blockade (C) are shown. MFI and percentage of NK cells expressing perforin, and granzyme B (D) and FasL and TRAIL (E) are shown. Mean with SEM shown for experimental replicates (n = 5). Two-tailed two-sample t-tests and one-way ANOVA with Kruskal-Wallis with Dunn's multiple comparisons tests were performed (* $p < 0.05$, ** $p < 0.01$).

Figure 4: AlloBMT and CD155 blockade with alloNK effectively treats relapsed OS pulmonary metastases. (A) Schematic showing K7M2 OS inoculation followed by alloBMT and alloNK infusion with CD155 axis blocking antibodies. (B) Serum levels of mouse IL-15/IL-15R pre- and post-BMT and alloNK and CD155 axis blockade treatment at timepoints post alloBMT (n = 6-15 mice per timepoint) (C) Overall survival for mice treated with alloBMT and alloNK with isotype control or anti-CD155 blockade are shown at timepoints post alloBMT (n = 8 or 10 mice per group). (D) Clinical GVHD scores for mice treated with alloBMT and alloNK with isotype control or anti-CD155 blockade are shown (n = 8 or 10 mice per group). (E) Bioluminescent total photon flux signal detected by IVIS and area under the curve are shown for mice treated with alloBMT and alloNK with isotype control or anti-CD155 blockade are shown at timepoints post tumor inoculation (n = 5 mice per group) (F) K7M2 OS bioluminescent total photon flux signal detected by IVIS shown for mice treated with alloBMT and alloNK with isotype control, anti-DNAM-1 blockade, anti-CD155 blockade, or anti-DNAM and anti-CD155 blockade are shown at timepoints post tumor inoculation (n = 5 mice per group). Bars and points with error bars depict mean with SEM. Log-rank test performed and student's t-tests were performed (* $p < 0.05$).

Figure 5: CD155 blockade with alloNK shows limited efficacy against established OS disease after alloBMT. (A) Schematic showing alloBMT, K7M2 OS inoculation and alloNK infusion with CD155 axis blocking antibodies. (B) Blood sera levels of mouse IL-15/IL-15R pre- and post-BMT and alloNK and CD155 axis blockade treatment (n = 7-8 per timepoint) (C) Overall survival for mice treated with alloBMT and alloNK with isotype control, anti-DNAM-1 blockade, anti-CD155 blockade, or anti-DNAM and anti-CD155 blockade are shown (n = 7 mice per group). (D) Clinical GVHD scores for mice treated with alloBMT and alloNK with isotype control, anti-DNAM-1 blockade, anti-CD155 blockade, or anti-DNAM and anti-CD155 blockade are shown (n = 7 mice per group). (E) K7M2 OS bioluminescent total photon flux signal detected by IVIS shown for mice treated with alloBMT and alloNK with isotype control, anti-DNAM-1 blockade, anti-CD155 blockade, or anti-DNAM and anti-CD155 blockade are shown (n = 7 mice per group). Bars and points with error bars depict mean with SEM.

Figure 6: CD155 blockade and DNAM-1 blockade with alloNK treatment changes gene expression in lung tissue of OS tumor-bearing mice post alloBMT. (A) Volcano plot shows distribution of significance ($-\log_{10}$(p-value)) and change in expression ($\log_2$Fold Change) of differentially expressed genes within the comparison of lung tissues from mice treated with CD155 blockade with alloNK cells and mice treated with isotype antibody and alloNK cells (n = 3 experimental replicates per group compared). All genes with absolute fold change ≥ 1.5 and p value ≤ 0.05 are plotted. Genes with absolute fold change ≥ 2 are labeled with upregulated genes represented by green dots and downregulated genes represented by red dots. (B) Genes with absolute fold change ≥ 2 are plotted with fold change and p values shown. (C) Nanostring gene set analysis of genes with absolute fold change ≥ 1.5 and p value ≤ 0.05 was performed. Pathways and directed global significance scores shown. (D) Volcano plot shows distribution of significance ($-\log_{10}$(p-value)) and change in expression ($\log_2$Fold Change) of differentially expressed genes within the comparison of lung tissues from mice treated with DNAM-1 blockade with alloNK cells and mice treated with isotype antibody and alloNK cells (n = 3 experimental replicates per group compared). All genes with absolute fold change ≥ 1.5 and p value ≤ 0.05 are plotted. Genes with absolute fold change ≥ 2 are labeled with upregulated genes represented by green dots and downregulated genes represented by red dots. (E) NK cell-related genes with absolute fold change ≥ 2 are plotted with fold change and p values shown. (F) T cell function-related genes with absolute fold change ≥ 2 are plotted with fold change and p values shown. (G) Nanostring gene set analysis of genes with absolute fold change ≥ 1.5 and p value ≤ 0.05 was performed. Pathways and directed global significance scores shown.

Figure 7: DNAM-1 blockade increases NKG2D expression in synNK and alloNK cells and has a greater impact on cytotoxicity compared to NKG2D. EAE murine alloNK and synNK were plated with K7M2 OS at an E:T ratio of 2.5:1. NK cells were collected and analyzed by flow cytometry. NKG2D MFI and percentage of NKG2D^{+} NK cells shown for (A) alloNK and synNK (B) synNK with anti-CD155, anti-DNAM-1, or anti-CD155 and anti-DNAM-1 blockade, and (C) alloNK with anti-CD155, anti-DNAM-1, or anti-CD155 and anti-DNAM-1 blockade. Mean with SEM shown for experimental replicates (n = 5). EAE murine alloNK and synNK were plated with mKate2-expressing K7M2 OS. %Lysis was calculated based on target alone and staurosporine-induced max lysis conditions. OS lysis shown for (D) alloNK and synNK with combinations of anti-CD155, anti-DNAM-1, and anti-NKG2D blockade at E: T 2.5:1 (n = 5 per group). Two-tailed two-sample t-tests and one-way ANOVA with Kruskal-Wallis with Dunn's multiple comparisons tests were performed (* $p < 0.05$, ** $p < 0.01$).

Supplementary Figure 1: EAE murine NK cells have increased expression of NKG2D, TNF death receptors, and CD155 receptors DNAM-1, CD96 and TIGIT. B6 (NK1.1+) and BALB/c ($CD49b^+$) NK cells were harvested and analyzed for expression of activating receptor DNAM-1 and inhibitory receptors CD96 and TIGIT by flow cytometry on days 0, 5, 7, 9, 12, and 14. DNAM-1 MFI and %$DNAM\text{-}1^+$, CD96 MFI and %$CD96^+$, and TIGIT MFI and %$TIGIT^+$ of (A) B6 and (B) BALB/c NK cells are shown. DNAM-1 MFI and %$DNAM\text{-}1^+$, CD96 MFI and %$CD96^+$, and TIGIT MFI and %$TIGIT^+$ of (C) B6 and (D) BALB/c NK cells are shown. Mean with SEM shown for experimental replicates (n = 5). One-way ANOVA and Kruskal-Wallis with Dunn's multiple comparisons tests were performed (* $p < 0.05$, ** $p < 0.01$, *** $p < 0.001$, **** $p > 0.0001$).

Supplementary Fig. 2: Degranulation is not significantly affected by CD155 or DNAM-1 blockade in synNK or alloNK cells against OS. EAE murine alloNK cells plated with K7M2 OS at an E:T ratio of 2.5:1. Cells were incubated for 30 minutes, followed by addition of monesin and brefeldin A, and incubated for an additional 4 hours. NK cells were collected, fixed and permeabilized, stained with surface and intracellular antibodies and analyzed by flow cytometry. Cells were gated on B6 (NK1.1^{+}) cells and CD107a, perforin, granzyme B, FasL, and TRAIL MFI were calculated. NK cells were further gated on CD107a^{+}, perforin^{+}, granzyme B^{+}, FasL^{+}, and TRAIL^{+} cells. MFI and percentage of synNK cells expressing CD107a, perforin, and granzyme B (A) and FasL and TRAIL (B) and alloNK cells expressing CD107a, perforin, and granzyme B (C) and FasL and TRAIL (D). Mean with SEM shown for experimental replicates (n = 5). One-way ANOVA with Kruskal-Wallis with Dunn's multiple comparisons tests were performed.

Supplementary Fig. 3 CD155 blockade increases human NK-92 cell-mediated lysis of CD155-expressing MG63 OS cell line. (A) Proportions of MG63 OS expressing CD155 and CD112 and (B) proportions of MG63 OS expressing only CD155, only CD112 or both CD155 and CD112 are shown. NK-92 cells were plated at a 1:1, 2:1, 5:1 and 7:1 E:T ratios with MG63 GFP^+ cells with or without anti-CD155 antibody. Mean and SEM shown for n=3 replicates per condition.

Figure 1.

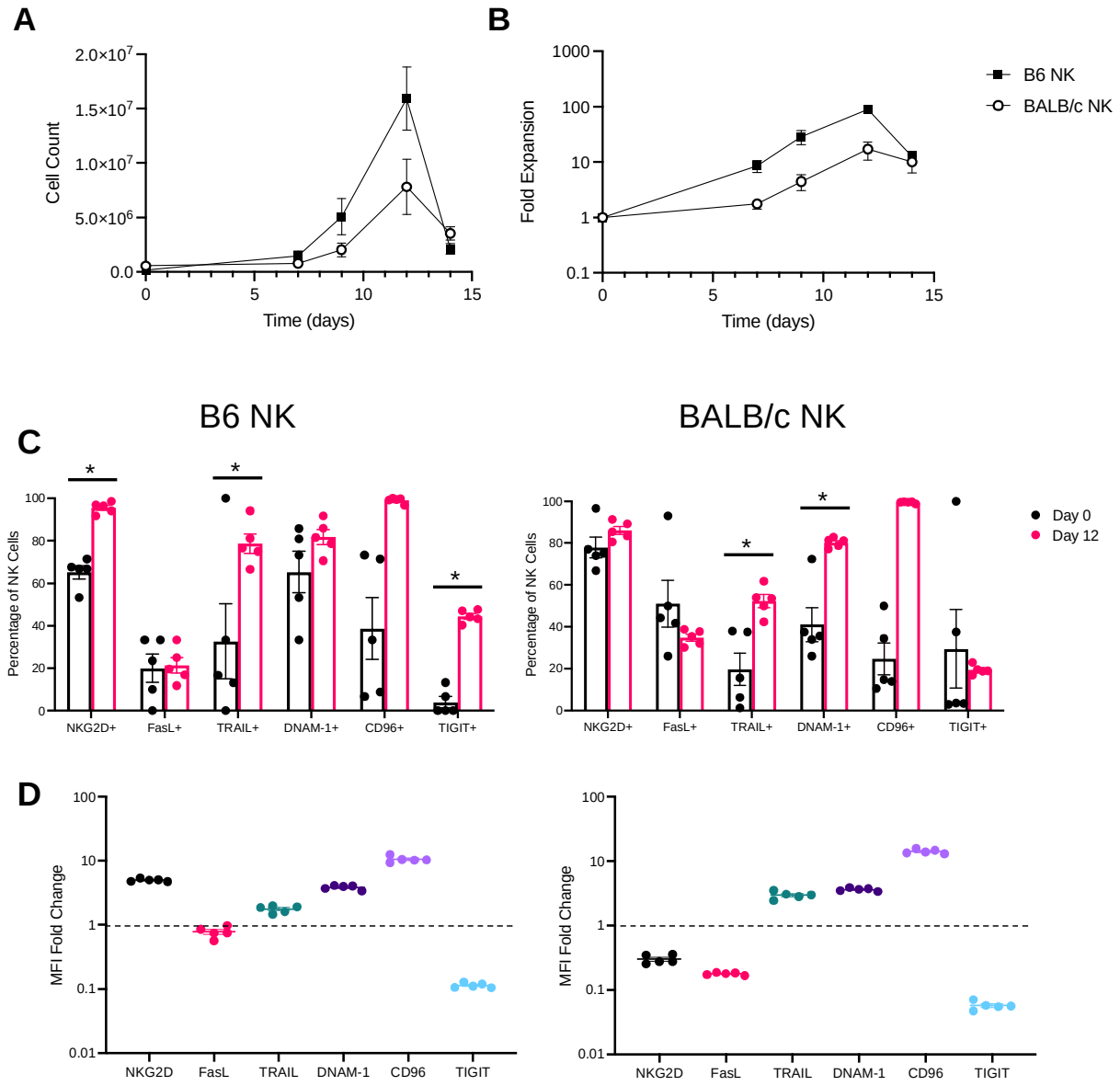
A
Cell Count
2.0×10^7
1.5×10^7
1.0×10^7
5.0×10^6
0.0
0
5
10
15
Time (days)
B
Fold Expansion
1000
100
10
1
0.1
0
5
10
15
Time (days)
B6 NK
BALB/c NK
C
B6 NK
BALB/c NK
Percentage of NK Cells
100
80
60
40
20
0
NKG2D+
FasL+
TRAIL+
DNAM-1+
CD96+
TIGIT+
*
Day 0
Day 12
D
MFI Fold Change
100
10
1
0.1
0.01
NKG2D
FasL
TRAIL
DNAM-1
CD96
TIGIT

Figure 2.

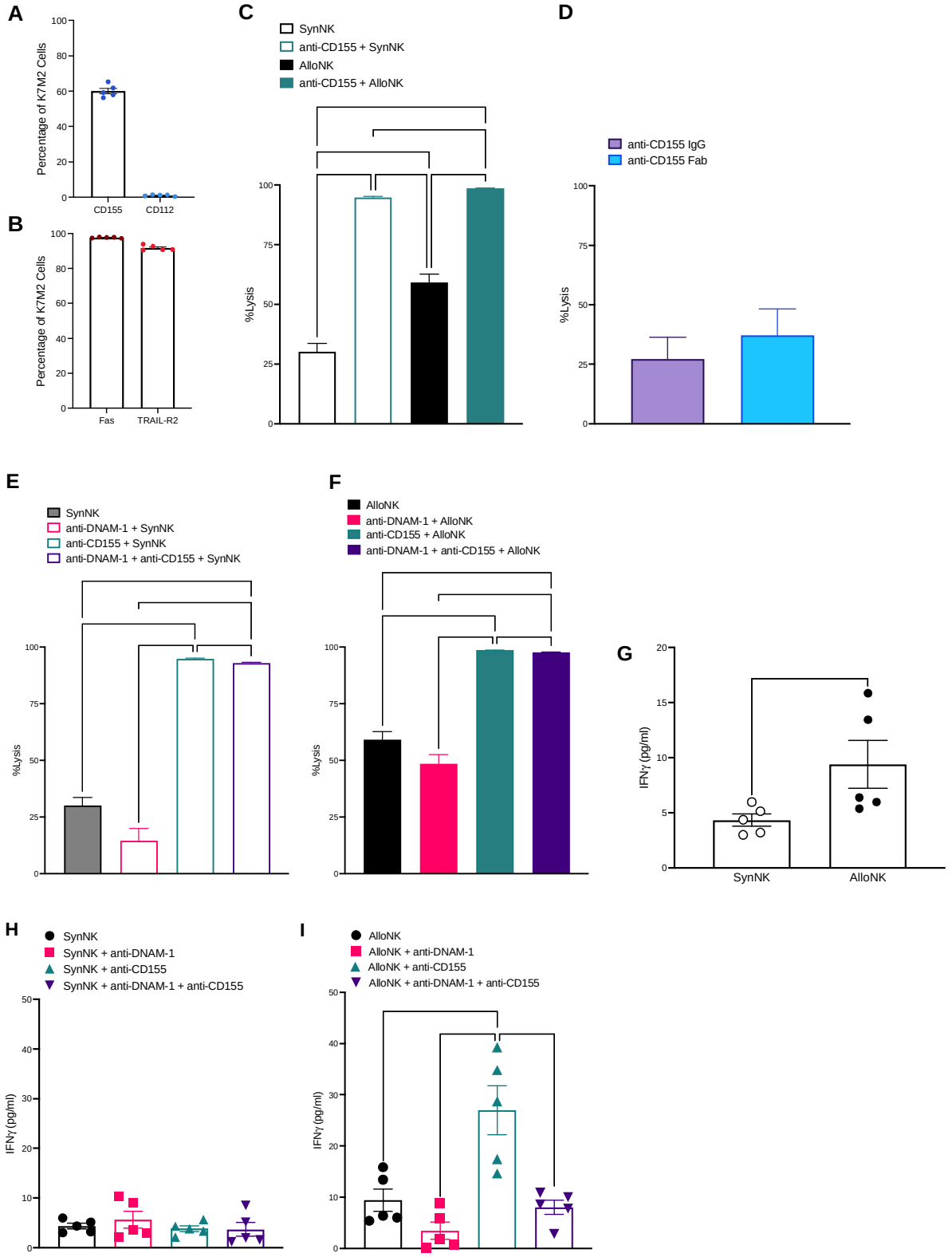
A
Percentage of K7M2 Cells
CD155
CD112
B
Percentage of K7M2 Cells
Fas
TRAIL-R2
C
SynNK
anti-CD155 + SynNK
AlloNK
anti-CD155 + AlloNK
%Lysis
D
anti-CD155 IgG
anti-CD155 Fab
%Lysis
E
SynNK
anti-DNAM-1 + SynNK
anti-CD155 + SynNK
anti-DNAM-1 + anti-CD155 + SynNK
%Lysis
F
AlloNK
anti-DNAM-1 + AlloNK
anti-CD155 + AlloNK
anti-DNAM-1 + anti-CD155 + AlloNK
%Lysis
G
IFNγ (pg/ml)
SynNK
AlloNK
H
SynNK
SynNK + anti-DNAM-1
SynNK + anti-CD155
SynNK + anti-DNAM-1 + anti-CD155
IFNγ (pg/ml)
I
AlloNK
AlloNK + anti-DNAM-1
AlloNK + anti-CD155
AlloNK + anti-DNAM-1 + anti-CD155
IFNγ (pg/ml)

Figure 3.

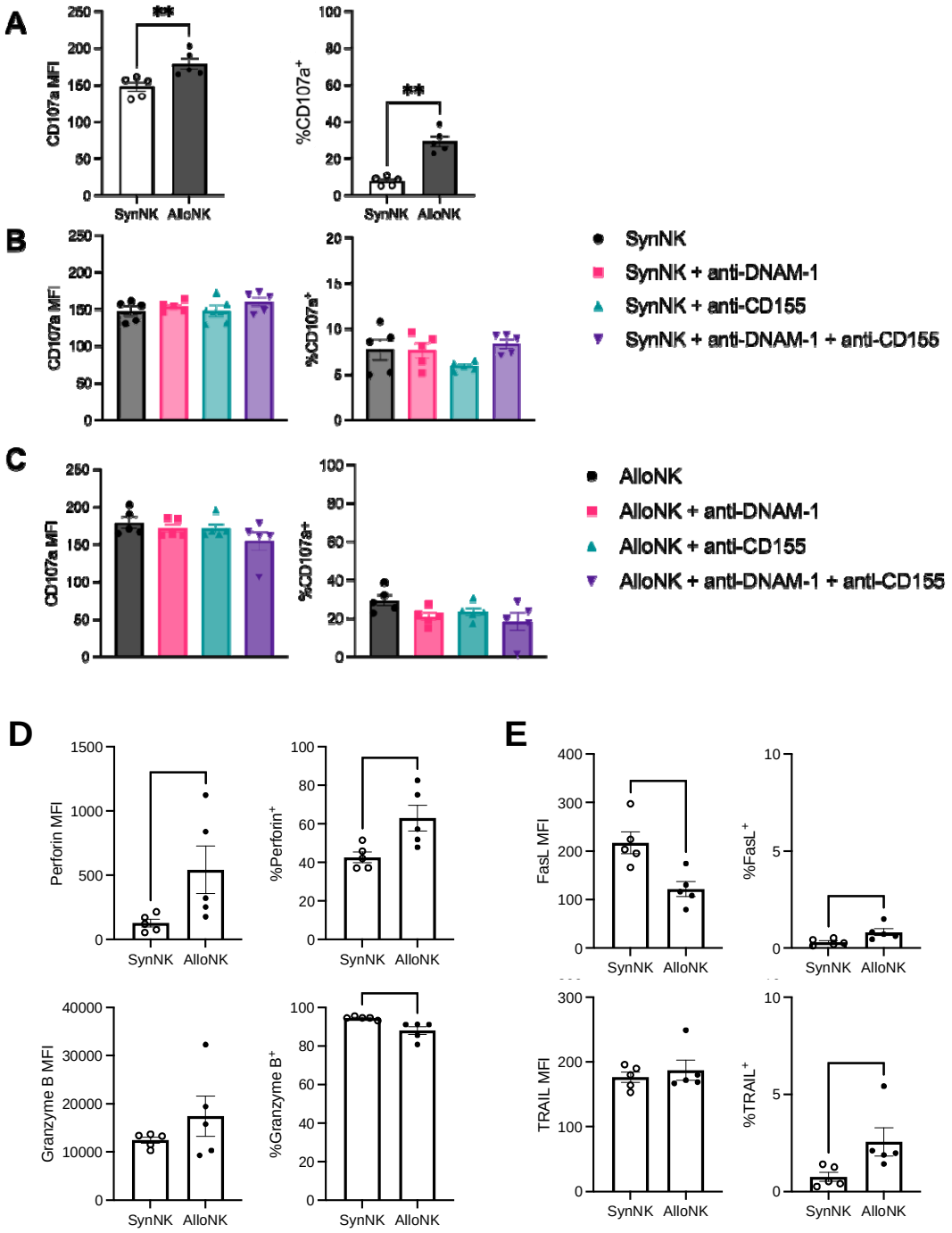
A
CD107a MFI
%CD107a+
SynNK
AlloNK
B
SynNK
SynNK + anti-DNAM-1
SynNK + anti-CD155
SynNK + anti-DNAM-1 + anti-CD155
C
AlloNK
AlloNK + anti-DNAM-1
AlloNK + anti-CD155
AlloNK + anti-DNAM-1 + anti-CD155
D
Perforin MFI
%Perforin+
Granzyme B MFI
%Granzyme B+
E
FasL MFI
%FasL+
TRAIL MFI
%TRAIL+

Figure 4.

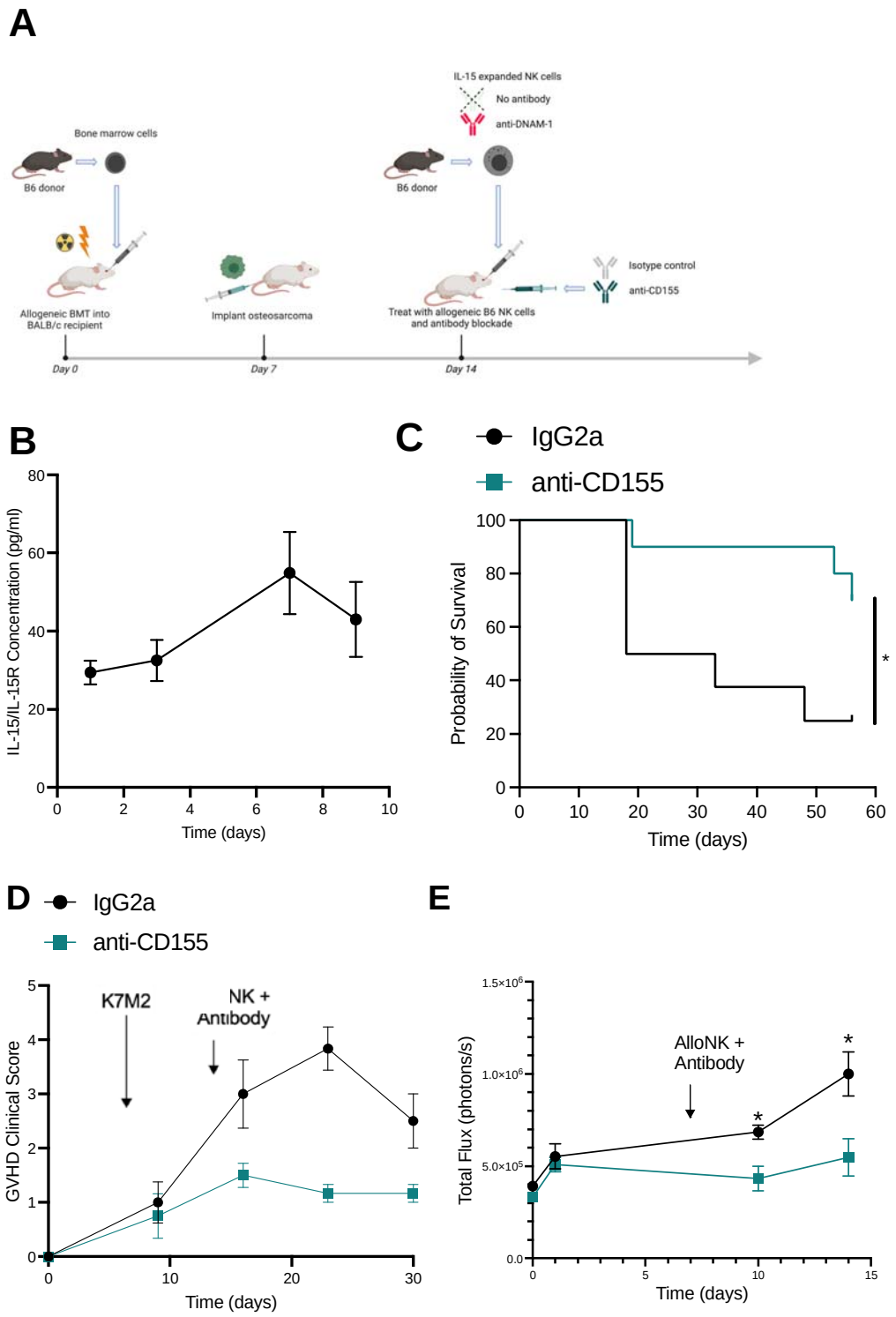
A
IL-15 expanded NK cells
No antibody
anti-DNAM-1
Bone marrow cells
B6 donor
B6 donor
Isotype control
anti-CD155
Allogeneic BMT into BALB/c recipient
Implant osteosarcoma
Treat with allogeneic B6 NK cells and antibody blockade
Day 0
Day 7
Day 14
B
IL-15/IL-15R Concentration (pg/ml)
Time (days)
C
IgG2a
anti-CD155
Probability of Survival
Time (days)
*
D
IgG2a
anti-CD155
K7M2
NK + Antibody
GVHD Clinical Score
Time (days)
E
AlloNK + Antibody
Total Flux (photons/s)
Time (days)
*
*

Figure 5.

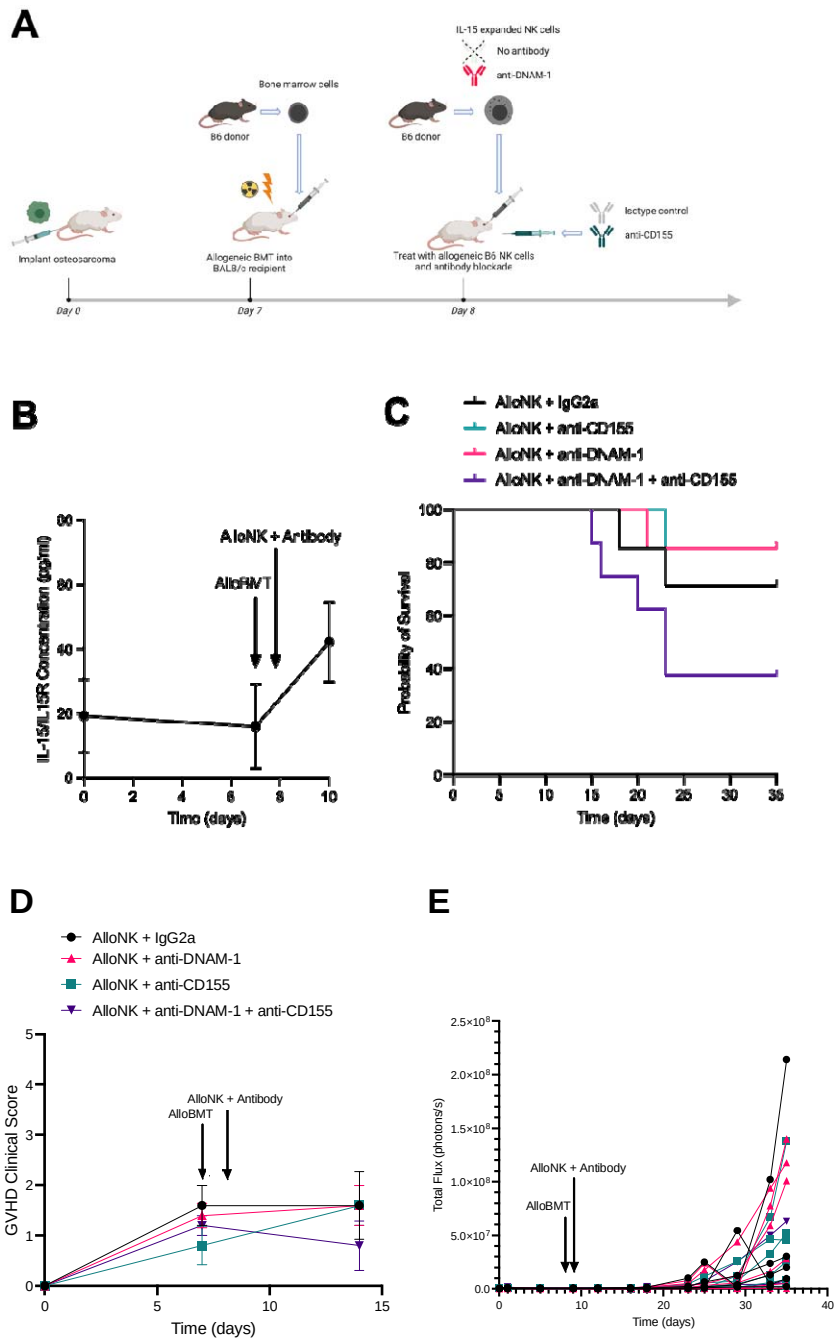
A
IL-15 expanded NK cells
No antibody
anti-DNAM-1
Bone marrow cells
B6 donor
B6 donor
Isotype control
anti-CD155
Implant osteosarcoma
Allogeneic BMT into BALB/c recipient
Treat with allogeneic B6 NK cells and antibody blockade
Day 0
Day 7
Day 8
B
AlloNK + Antibody
AlloBMT
IL-15/IL15R Concentration (pg/ml)
Time (days)
C
AlloNK + IgG2a
AlloNK + anti-CD155
AlloNK + anti-DNAM-1
AlloNK + anti-DNAM-1 + anti-CD155
Probability of Survival
Time (days)
D
AlloNK + IgG2a
AlloNK + anti-DNAM-1
AlloNK + anti-CD155
AlloNK + anti-DNAM-1 + anti-CD155
AlloNK + Antibody
AlloBMT
GVHD Clinical Score
Time (days)
E
AlloNK + Antibody
AlloBMT
Total Flux (photons/s)
Time (days)

Figure 6.

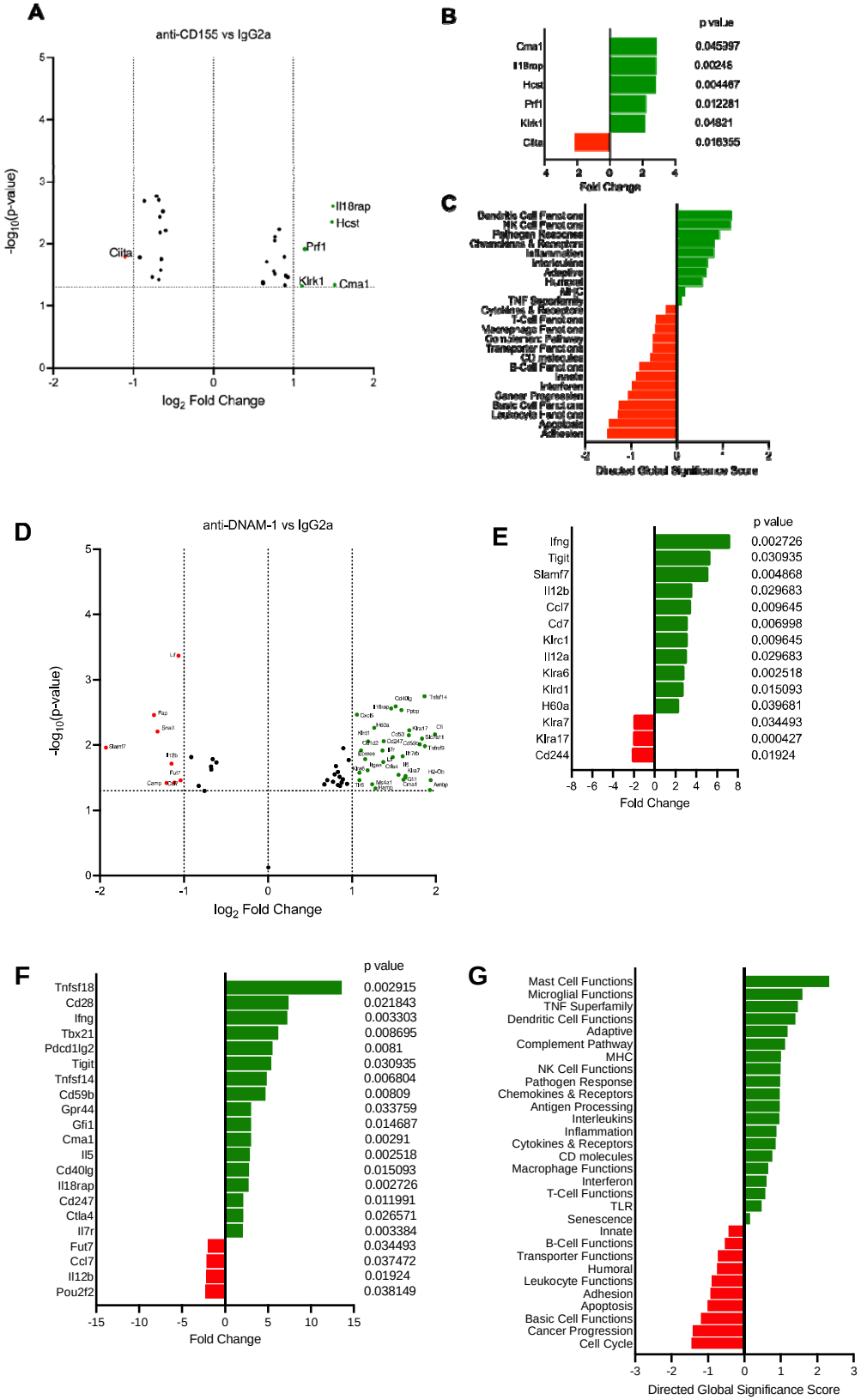
A
anti-CD155 vs IgG2a
-log10(p-value)
log2 Fold Change
Ciita
Il18rap
Hcst
Prf1
Klrk1
Cma1
B
p value
Cma1 0.045397
Il18rap 0.00246
Hcst 0.004467
Prf1 0.012281
Klrk1 0.04821
Ciita 0.016355
Fold Change
C
Directed Global Significance Score
D
anti-DNAM-1 vs IgG2a
-log10(p-value)
log2 Fold Change
E
p value
Ifng 0.002726
Tigit 0.030935
Slamf7 0.004868
Il12b 0.029683
Ccl7 0.009645
Cd7 0.006998
Klrc1 0.009645
Il12a 0.029683
Klra6 0.002518
Klrd1 0.015093
H60a 0.039681
Klra7 0.034493
Klra17 0.000427
Cd244 0.01924
Fold Change
F
p value
Tnfsf18 0.002915
Cd28 0.021843
Ifng 0.003303
Tbx21 0.008695
Pdcd1lg2 0.0081
Tigit 0.030935
Tnfsf14 0.006804
Cd59b 0.00809
Gpr44 0.033759
Gfi1 0.014687
Cma1 0.00291
Il5 0.002518
Cd40lg 0.015093
Il18rap 0.002726
Cd247 0.011991
Ctla4 0.026571
Il7r 0.003384
Fut7 0.034493
Ccl7 0.037472
Il12b 0.01924
Pou2f2 0.038149
Fold Change
G
Mast Cell Functions
Microglial Functions
TNF Superfamily
Dendritic Cell Functions
Adaptive
Complement Pathway
MHC
NK Cell Functions
Pathogen Response
Chemokines & Receptors
Antigen Processing
Interleukins
Inflammation
Cytokines & Receptors
CD molecules
Macrophage Functions
Interferon
T-Cell Functions
TLR
Senescence
Innate
B-Cell Functions
Transporter Functions
Humoral
Leukocyte Functions
Adhesion
Apoptosis
Basic Cell Functions
Cancer Progression
Cell Cycle
Directed Global Significance Score

Figure 7.

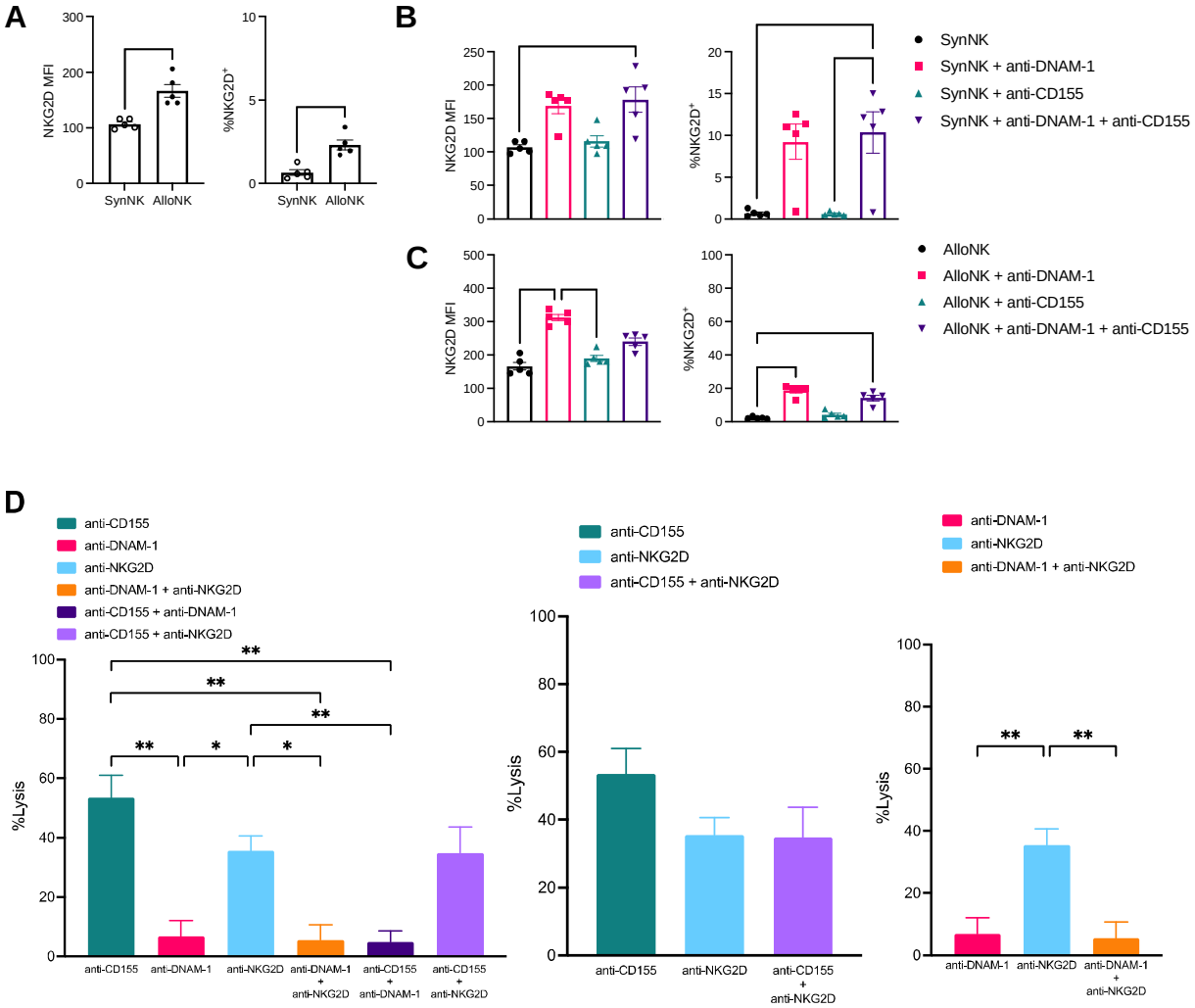
A
NKG2D MFI
%NKG2D+
SynNK
AlloNK
B
SynNK
SynNK + anti-DNAM-1
SynNK + anti-CD155
SynNK + anti-DNAM-1 + anti-CD155
C
AlloNK
AlloNK + anti-DNAM-1
AlloNK + anti-CD155
AlloNK + anti-DNAM-1 + anti-CD155
D
anti-CD155
anti-DNAM-1
anti-NKG2D
anti-DNAM-1 + anti-NKG2D
anti-CD155 + anti-DNAM-1
anti-CD155 + anti-NKG2D
%Lysis
anti-CD155 + anti-NKG2D
anti-DNAM-1 + anti-NKG2D

Supplementary Figure 1.

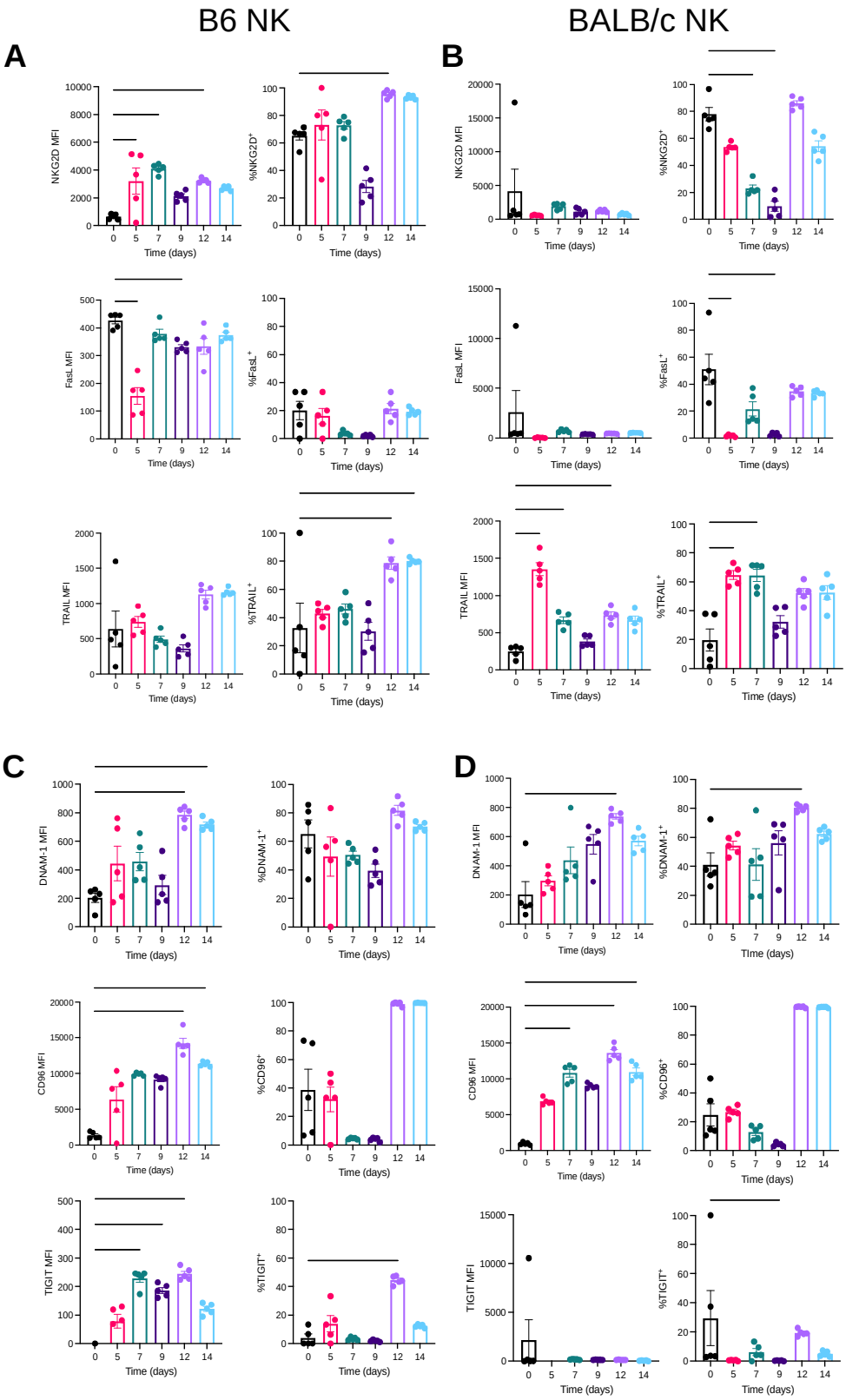

Supplementary Figure 2.

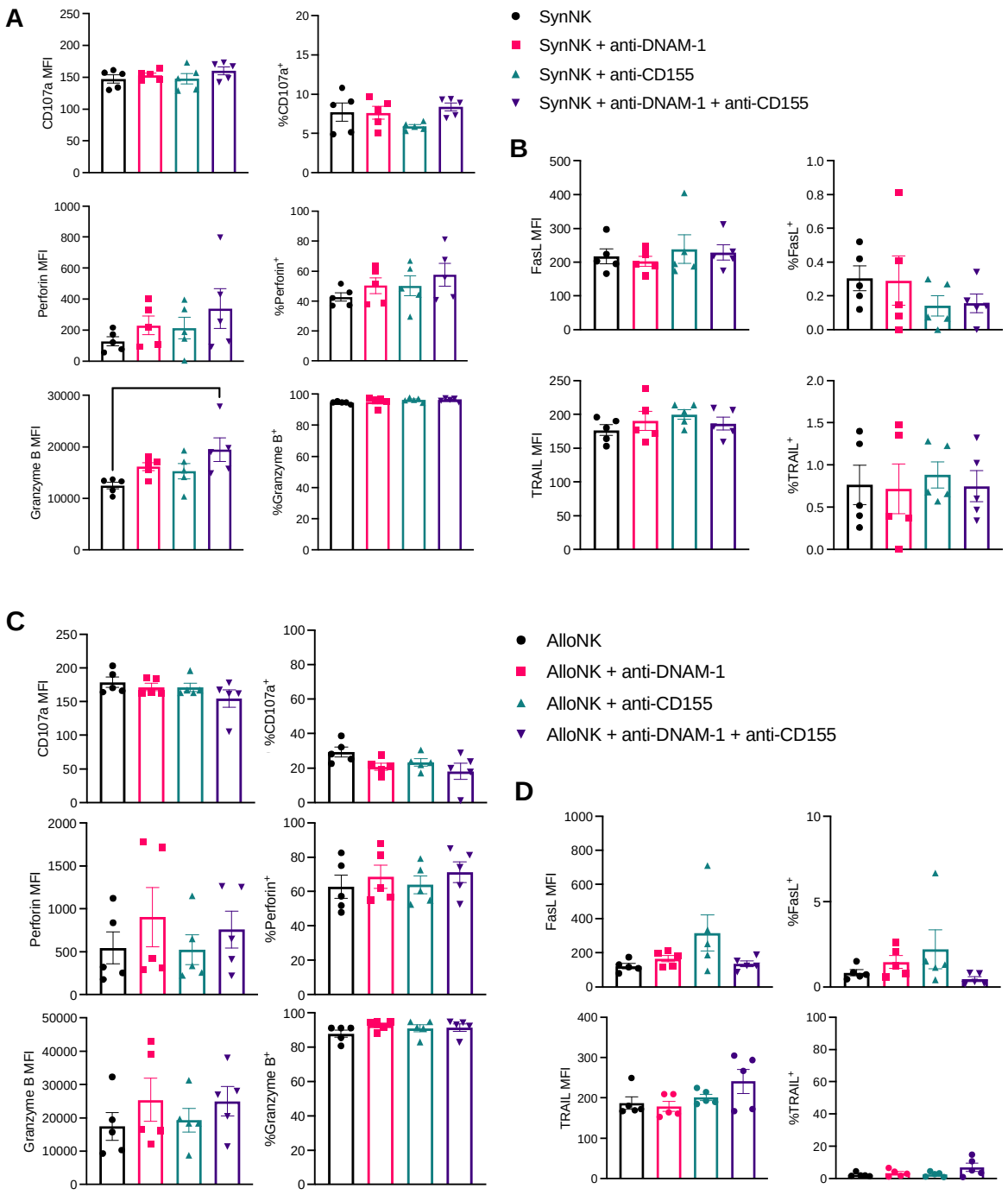
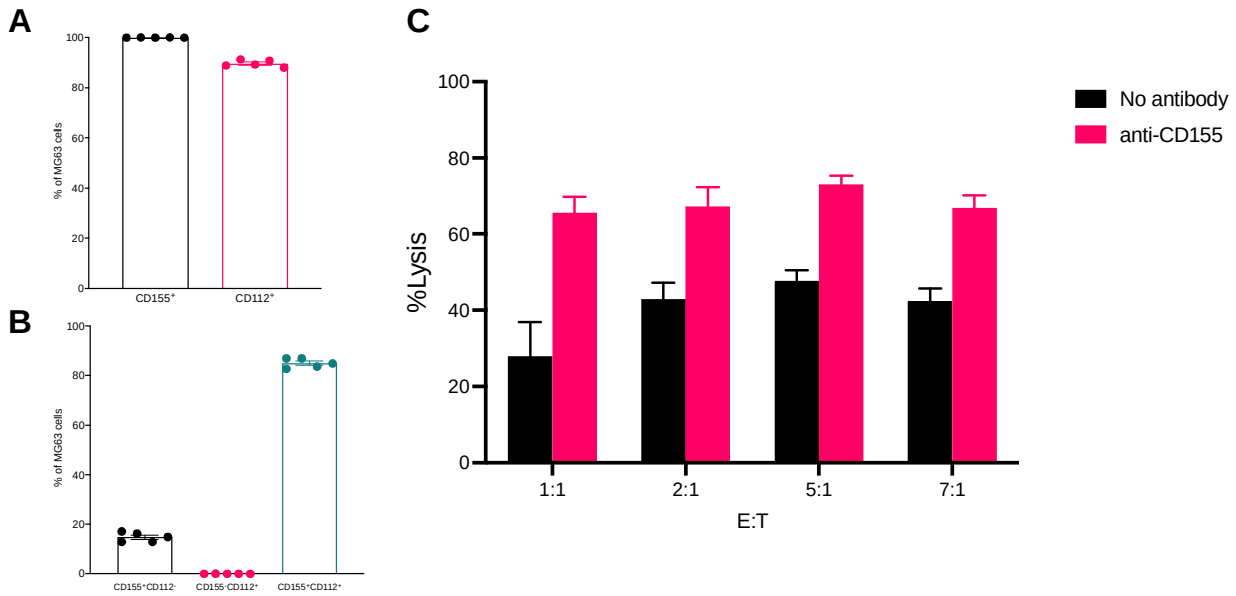
Supplementary Figure 3.